Geochemistry Geophysics Geosystems G3
AN ELECTRONIC JOURNAL OF THE EARTH SCIENCES
Published by AGU and the Geochemical Society

Article
Volume 6, Number 5
12 May 2005
Q05L09, doi:10.1029/2004GC000875
ISSN: 1525-2027

Petrogenesis of Hawaiian postshield lavas: Evidence from Nintoku Seamount, Emperor Seamount Chain

John T. Shafer and Clive R. Neal
Department of Civil Engineering and Geological Science, University of Notre Dame, 156 Fitzpatrick Hall, Notre Dame, Indiana 46615, USA (jshafer@nd.edu)

Marcel Regelous
Department of Earth Sciences, University of Bristol, Bristol, UK

Max Planck Institut für Chemie, Postfach 3060, Mainz 55020, Germany

[1] We report major and trace element and Sr and Nd isotope data for a 283 m thick sequence of postshield lavas drilled during Ocean Drilling Project Leg 197 from Site 1205, Nintoku Seamount, an approximately 56 m.y. old volcano from the Emperor Seamount Chain. At least 25 subaerially erupted lava flow units were sampled, of which all but one are alkali basalts. Clasts of hawaiite and mugearite are present in a conglomerate overlying the basement sequence. Similar rock types characterize the postshield stage of many young Hawaiian volcanoes. Major and trace element, and age-corrected Sr and Nd isotope compositions of the Nintoku lavas are similar to those of young postshield lavas from the Hawaiian Islands. Concentrations of highly incompatible elements tend to increase, La/Yb and Nb/Zr ratios increase, and $^{87}Sr/^{86}Sr$ decreases with decreasing depth in the drill core. The more evolved rock types can be related to the underlying alkali basalts by fractional crystallization of olivine, clinopyroxene, plagioclase, and Fe-Ti oxides, all of which occur as phenocryst or significant groundmass phases in these lavas. However, variations in the trace element and isotopic compositions of the Nintoku lavas indicate derivation from a heterogeneous mantle source. The isotopic and trace element compositions of the lavas can be modeled using a modified version of the Chen and Frey (1985) mixing model for Hawaiian lavas, in which small-degree melts of the ~60 m.y. old oceanic lithosphere beneath Nintoku, previously fertilized by small-degree melts soon after its formation at a ridge axis, are mixed with melts from the Hawaiian plume. The contribution from the oceanic lithosphere became more important with time as Nintoku Seamount moved away from the Hawaiian plume axis. Together with other data from Leg 197, our results show that the $^{87}Sr/^{86}Sr$ ratios of not only shield but also postshield lavas from the Emperor Seamounts increased with decreasing age between ~80 and 50 m.y. ago. For alkalic postshield lavas, this could result from either increased melting of the oceanic lithosphere beneath volcanoes situated on younger oceanic crust or lower degrees of incompatible trace element enrichment in the lowermost portions of younger oceanic lithosphere.

Components: 15,107 words, 16 figures, 7 tables.

Index Terms: 1040 Geochemistry: Radiogenic isotope geochemistry; 3619 Mineralogy and Petrology: Magma genesis and partial melting (1037); 3640 Mineralogy and Petrology: Igneous petrology.

Received 29 October 2004; **Revised** 22 February 2005; **Accepted** 14 March 2005; **Published** 12 May 2005.

Shafer, J. T., C. R. Neal, and M. Regelous (2005), Petrogenesis of Hawaiian postshield lavas: Evidence from Nintoku Seamount, Emperor Seamount Chain, *Geochem. Geophys. Geosyst.*, *6*, Q05L09, doi:10.1029/2004GC000875.

Theme: Movement, Dynamics, and Geochemical Evolution of the Hawaiian Hotspot
Guest Editors: R. Duncan, J. A. Tarduno, D. Scholl, and T. Davies

1. Introduction

[2] The intraplate Hawaiian Ridge-Emperor Seamount Chain is an approximately 6,000 km long, age-progressive chain of volcanic islands and seamounts that has been created as the Pacific plate moved over the Hawaiian hot spot (Figure 1). Active volcanism occurs on the Hawaiian Islands at the eastern end of the Hawaiian Ridge and the volcanoes become progressively older to the west and north. The oldest preserved volcanoes, at the northern end of the Emperor Seamount Chain (ESC) at Meiji and Detroit Seamount, have an age of approximately 76–80 Ma [*Keller et al.*, 1995; *Duncan and Keller*, 2004]. Lavas from the ESC thus preserve a record of Hawaiian hot spot geochemistry since the Late Cretaceous. The Emperor Seamount Chain is built on Pacific lithosphere ranging in age from about 80 to less than 10 million years older than the central volcanoes [*Mammerickx and Sharman*, 1988], providing a opportunity to examine the role of the thickness and fertility of the lithosphere on the chemistry of intraplate magmatism. Hawaiian postshield lavas are believed to be derived in part from the oceanic lithosphere [e.g., *Chen and Frey*, 1983; *Reiners and Nelson*, 1998; *Yang et al.*, 2003].

[3] Recent studies have shown that the geochemistry of lavas from the ESC vary dramatically from one end to the other. Tholeiitic and alkalic lavas from Meiji and Detroit Seamounts are depleted in highly incompatible trace elements compared to their younger counterparts from the Hawaiian Islands [*Keller et al.*, 2000; *Regelous et al.*, 2003]. Initial $^{87}Sr/^{86}Sr$ ratios of tholeiitic and alkalic lavas from Detroit and Meiji Seamounts (5580 and 5800 km from Kilauea, respectively) extend to lower values than lavas from younger Hawaiian-Emperor Seamounts [*Keller et al.*, 2000; *Regelous et al.*, 2003; *Huang et al.*, 2005]. The depleted compositions of the oldest Emperor lavas could reflect the fact that these seamounts were formed on young, thin lithosphere close to a former spreading center [*Mammerickx and Sharman*, 1988]. For example, the composition of Detroit Seamount lavas may be a consequence of magma mixing between MORB and OIB melts [*Kinman and Neal*, 2002], increased entrainment of depleted upper mantle into the Hawaiian plume, or partial melting of depleted upper mantle close to the ridge [*Keller et al.*, 2000], or be the result of higher average degrees of melting beneath thin lithosphere resulting in an increased contribution of relatively refractory, incompatible trace element depleted mantle components [*Regelous et al.*, 2003; *Frey et al.*, 2005; *Ito and Mahoney*, 2005a, 2005b].

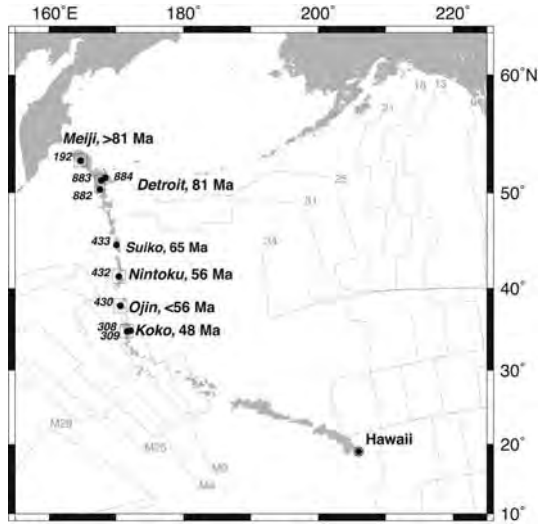

Figure 1. Map of the Hawaiian Ridge-Emperor Seamount Chain and surrounding area. Modified from *Tarduno et al.* [2002]. Shaded are regions of seafloor extending above approximately 3500 mbsl.

[4] In contrast, the available geochemical data for lavas from younger Emperor Seamounts (between Suiko and Daikakuji, 65–42 Ma) show that these seamounts have major and trace element compositions similar to those of young Hawaiian lavas [*Clague and Dalyrmple*, 1973; *Dalrymple and Clague*, 1976; *Bence et al.*, 1980; *Clague and Frey*, 1980; *Dalrymple and Garcia*, 1980; *Kirkpatrick et al.*, 1980; *Keller et al.*, 2000; *Regelous et al.*, 2003]. However, with the exception of Suiko Seamount, samples from the younger Emperor Seamounts are limited to a few dredge and shallow drill sites. Dredged samples in particular are generally highly altered, so the primary geochemistry of lavas from most of these seamounts is poorly known.

[5] The subaerial Hawaiian Islands afford a detailed look at the evolution of volcanoes produced by the Hawaiian hot spot. Most young volcanoes pass through a series of evolutionary stages. Preshield volcanism is small in volume and predominantly alkalic in composition and is followed by voluminous amounts of tholeiitic basalt that erupt to form the bulk of the shield. After a short period of quiescence, postshield alkali basalts and their differentiates are erupted and form a thin discontinuous cap (<1% of total volcano volume) over the tholeiitic base [*Powers*, 1955; *Macdonald and Katsura*, 1964; *Engel et al.*, 1965; *Clague and*

Beeson, 1980]. In some cases, postshield alkali basalts have been found intercalated with tholeiitic basalts. Occasionally, renewed volcanism at isolated vents may occur up to 2.5 m.y. after eruption of the postshield basalts. These so-called posterosional lavas are strongly alkalic and comprise <0.1% of the total volcano volume. Not all stages are developed on all volcanoes, for example, Koolau and Lanai volcanoes lack a postshield alkalic stage. Compared to the associated shield tholeiites, the younger alkalic lavas have higher concentrations of incompatible trace elements, higher ratios of more to less incompatible elements (e.g., Nb/Zr, La/Yb), and extend to silica undersaturated compositions.

[6] In this study, we report major and trace element and Sr and Nd isotope data for 33 samples of volcanic rock from a 283 m thick sequence of alkalic postshield lavas drilled from Nintoku Seamount during Ocean Drilling Program (ODP) Leg 197, Site 1205. The relatively thick, stratigraphically controlled sequence of postshield lavas at Nintoku provides an opportunity to examine the evolution of the Hawaiian plume through geochemical variability of ~56 Ma postshield lavas, and compare them to present-day postshield basalt compositions.

2. Nintoku Seamount

[7] Nintoku Seamount is located at 41°N, 175°E in the central part of the ESC, and formed at approximately 56 Ma [*Dalrymple et al.*, 1980; *Duncan and Keller*, 2004]. The upper 32 m of the volcanic basement of this seamount was previously drilled during Deep Sea Drilling Project (DSDP) Leg 55, Site 432, where three flow units of alkali basalt were recovered [*Kirkpatrick et al.*, 1980]. Site 1205 of ODP Leg 197 is located at the north-west edge of the summit region of Nintoku Seamount in 1310 m water depth, about 100 m south-west of Site 432. Hole 1205A encountered basement at 42.7 meters below seafloor (mbsf) and penetrated 283.3 m into a sequence of basaltic lavas and interbedded sediments and soil horizons (Figure 2). The minimum age of the basement rocks at this site is constrained to be 53.6–54.7 Ma on the basis of the nanofossil assemblage (zone NP10, Early Eocene) recovered in Core 197-1205A-5R immediately overlying volcanic basement. *Dalrymple et al.* [1980] obtained an ^{40}Ar-^{39}Ar age of 56.2 ± 0.6 Ma for a sample of olivine and plagioclase phyric alkali basalt from DSDP Site 432. ^{40}Ar-^{39}Ar plateau ages from 6 whole rock samples and one feldspar separate from Site 1205 gave a mean age of 55.51 ± 0.22 Ma [*Duncan and Keller*, 2004], with no significant difference in age between samples from the top and bottom of the section.

[8] At least 25 lava flow units were recovered at Site 1205. These included both a'a and pahoehoe flow types, which were commonly vesicular and have weathered flow top and inter-flow soil horizons indicating that the sequence was erupted subaerially and that eruption rates were relatively low [*Tarduno et al.*, 2002].

[9] The lavas drilled at Site 1205 vary from aphyric to plagioclase-phyric to plagioclase-olivine-phyric basalts with texture varying from subophitic to subtrachytic [*Tarduno et al.*, 2002]. The groundmass is typically composed of plagioclase, olivine, clinopyroxene, titanomagnetite, and glass. Preliminary shipboard major element analyses of the lava flow units showed that most are composed of alkali basalt. A conglomerate containing clasts of alkali basalt, hawaiite, and mugearite overlies the basement at Sites 1205 and 432. Alkali basalts and hawaiites with similar chemistry and mineralogy characterize the postshield alkalic stage of many young Hawaiian volcanoes, including Mauna Kea [*Frey et al.*, 1990], Kohala [*Lanphere and Frey*, 1987], and Haleakala [*Chen et al.*, 1990].

3. Samples and Analytical Methods

[10] A total of 33 samples were analyzed (Table 1). Of these, six samples are clasts of volcanic rock that were extracted from the conglomerate unit directly overlying the volcanic basement. Drill-core samples were crushed to 0.5–1.0 cm sized chips and the freshest material was handpicked. Vesicle fillings, veins, and highly altered material were avoided. The chips were rinsed in distilled water, dried, and powdered in an agate swing mill at the Max Planck Institut fur Chemie, Mainz.

[11] Loss on ignition (LOI) was determined by heating between 0.1 and 0.5 g of sample powder in platinum crucibles at 1025°C for 4 hours. The samples were weighed before and after removal from the oven and total weight percent LOI was determined.

[12] Major element concentrations were determined by inductively coupled plasma-optical emission spectroscopy (ICP-OES) at the University of Notre Dame. Approximately 0.1 g of sample powder was fused with 0.5 g of lithium

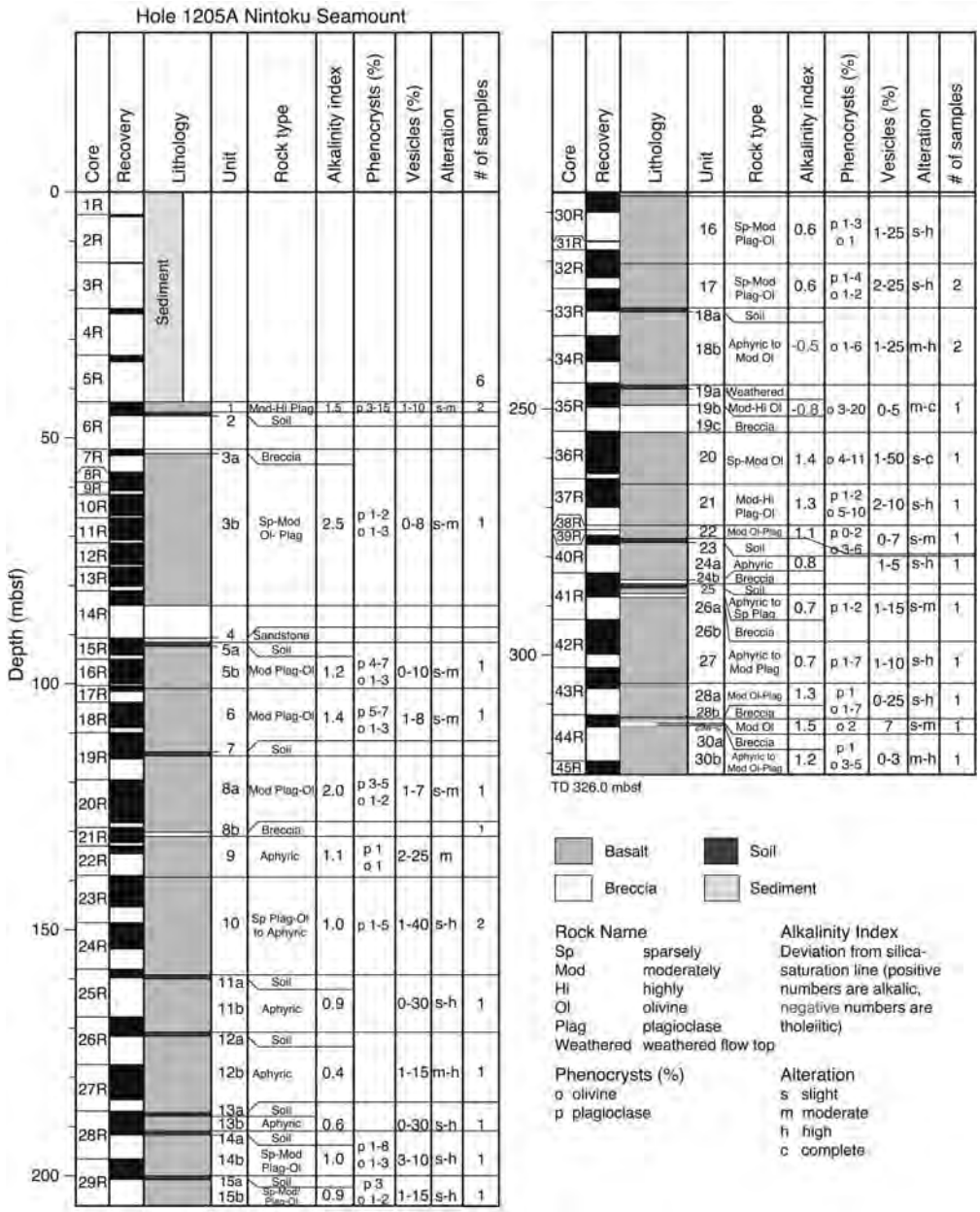

Figure 2. Stratigraphic profile for Hole 1205A Nintoku Seamount, listing thickness, mineralogy, and petrology of volcanic units. Adapted from *Tarduno et al.* [2002].

metaborate in carbon crucibles at 1025°C for 30 minutes in a Fisher Scientific Isotemp programmable muffle furnace. Immediately upon removal from the oven, the molten pellets were quenched in 5% HNO_3, which was then transferred to polypropylene bottles and brought to 100 g with 5% HNO_3. This solution was then placed in an ultrasonic bath until the fused glass was completely dissolved. This solution was then used for ICP-OES analyses. Machine drift was monitored by analyzing a standard solution every four samples (i.e., every four test tubes). Calibration was performed by taking the blank- and drift-corrected counts of a selected standard reference material, or SRM (two or three different SRMs were replicated at least twice during each run including BHVO-1, BHVO-2, BIR-1, and BPL-1), and dividing by the accepted elemental concentrations [*Shafer et al.*, 2004]. The background signal (the raw counts per second or cps) for the analytical blanks were generally low (<0.8% of standard reference material cps, except for P_2O_5, which

Table 1. Summary of Unit Number, Recovery Depth, and Rock Type of Samples Recovered From Hole 1205A

Sample	Unit Number	Depth, mbsf	Rock Type
5R-2, 21–25	SE II	34.09	mugearite
5R-2, 31–34	SE II	34.19	mugearite
5R-2, 74–77	SE II	34.62	mugearite
5R-2, 90–94	SE II	34.78	alkalic basalt
5R-2, 96–100	SE II	34.84	mugearite
5R-2, 114–116	SE II	35.02	hawaiite
6R-2, 8–12	1	43.88	moderately to highly plagioclase-phyric basalt
6R-2, 114–119	1	45.02	moderately to highly plagioclase-phyric basalt
10R-2, 0–5	3B	63.12	sparsely to moderately olivine-plagioclase-phyric basalt
15R-3, 10–12	5B	93.65	moderately plagioclase-olivine-phyric basalt
19R-1, 80–86	6	110.70	moderately plagioclase-olivine-phyric basalt
20R-5, 67–72	8A	125.80	moderately plagioclase-olivine-phyric basalt
21R-3, 71–76	8B	132.83	plagioclase-olivine basalt autoclastic breccia
23R-1, 85–90	10	139.75	sparsely plagioclase-olivine-phyric to aphyric basalt
24R-1, 51–56	10	149.01	sparsely plagioclase-olivine-phyric to aphyric basalt
26R-2, 30–34	11B	169.50	aphyric basalt
27R-6, 124–129	12B	185.66	aphyric basalt
28R-3, 10–15	13B	189.75	aphyric basalt
29R-3, 92–95	14B	199.01	sparsely to moderately plagioclase-olivine-phyric basalt
29R-4, 117–121	15B	201.30	sparsely to moderately plagioclase-olivine-phyric basalt
32R-3, 17–22	17	220.47	sparsely to moderately plagioclase-olivine-phyric basalt
33R-2, 70–75	17	226.61	sparsely to moderately plagioclase-olivine-phyric basalt
34R-3, 79–84	18B	238.29	aphyric to moderately olivine-phyric basalt
35R-3, 108–114	19B	247.66	moderately to highly olivine-phyric basalt
36R-5, 135–139	20	260.44	sparsely to moderately olivine-phyric basalt
37R-5, 38–42	21	270.02	moderately to highly plagioclase-olivine-phyric basalt
38R-1, 4–7	22	273.64	moderately olivine-plagioclase-phyric basalt
41R-3, 18–23	24B	285.02	aphyric basalt breccia
41R-5, 46–50	26A	288.24	aphyric to sparsely plagioclase-phyric basalt
42R-4, 12–16	27	296.96	aphyric to sparsely plagioclase-phyric basalt
44R-2, 14–19	28	313.34	olivine-plagioclase basalt breccia
44R-2, 116–121	29A	314.36	olivine basalt breccia
45R-1, 115–118	30B	322.65	aphyric to moderately olivine-plagioclase-phyric basalt

ranged from 11–48% of the reference material cps).

[13] Trace element abundances of the agate-milled powders were quantified by ICP-mass spectrometry (ICP-MS) using a PlasmaQuad II quadrupole machine at the University of Notre Dame [*Neal*, 2001]. Blank levels were around 100 cps for the REE and the standard deviation for replicated SRMs was generally less than 10% (REE < 5%, except for Yb and Er). In all ICP analyses, dissolution was performed on unignited powders.

[14] Strontium and Nd isotope analyses were carried out at Bristol University. Before dissolution, sample powders designated for Sr isotope analysis were subjected to a sequential leaching procedure in order to remove alteration products. About 4 g of rock powder was weighed into a Teflon beaker to which 5–10 ml of distilled 6M HCl was added. The samples were placed in an ultrasonic bath for 2 hours and the acid was changed every 30 minutes. The samples were then leached in hot (80°C) 6M HCl for a further 5 hours with the acid being changed every 60 minutes. The residue was soaked in deionized water at 80°C for 30 minutes, rinsed twice, and dried. This leaching procedure has been shown to yield reliable initial Sr isotope data for old, altered Hawaiian lavas [see *Regelous et al.*, 2003; *Huang et al.*, 2005].

[15] For Sr isotope analysis, about 0.1 g of leached rock powder was spiked with ^{87}Rb and ^{84}Sr and digested in HF-HNO_3. After treating with 15M HNO_3 and 6M HCl, the sample was dissolved completely in dilute HCl. Rubidium and Sr were separated from the rock matrix on cation exchange columns in 2.5M HCl. The Rb fraction was evaporated to dryness, redissolved in 3M HNO_3, and cleaned of Sr by passing it through a second column containing 50 μl of Sr Spec resin.

[16] Neodymium isotope analyses were conducted on unleached sample powders. Approximately 0.1 g of rock powder was digested using HF-HNO_3-HCl, dissolved in 3M HNO_3, and passed through a column containing 0.1 ml of exchange resin. After washing with 3M HNO_3, the rare earth elements (REE) were recovered in 2.5M HCl. Neodymium was separated from the other REE using HDEHP columns and dilute HCl. All reagents used were quartz distilled and total procedural blanks for Sr and Nd were below 400 pg and 50 pg, respectively.

[17] Strontium and Nd isotope measurements were conducted using a Finnigan "Triton" thermal ionization mass spectrometer in static mode. These measurements were corrected for instrumental mass fractionation using exponential fractionation corrections and assuming $^{86}Sr/^{88}Sr = 0.1194$ and $^{146}Nd/^{144}Nd = 0.7219$. The NBS-987 Sr and J&M Nd standards gave 0.710247 ± 8 (n = 12) and 0.511114 ± 5 (n = 8), respectively, over the period of the analysis.

[18] Rubidium isotope compositions were determined by multicollector ICP-MS using methods adapted from *Waight et al.* [2002]. The Rb fraction was dissolved in 0.6M HCl + 0.02M HF in order to obtain a Rb concentration of ~100 ppb. About 2 ml of this solution was transferred to a small vial and approximately 250 ng of natural Zr was added. Sample solutions were introduced into a Finnigan "Neptune" double focusing MC-ICP-MS via a Cetac Aridus microconcentric nebulizer and desolvating system equipped with a PFA spray chamber, at an uptake rate of 50 μl/minute. Typical sensitivity for Rb was ~200–400 Volts/ppm. Masses 85, 87, 88, 90, and 91 were measured simultaneously on Faraday cups. The contribution of Sr to mass 87 was monitored via mass 88 and in all cases the correction applied (using the $^{88}Sr/^{87}Sr$ ratio obtained for individual samples by TIMS) was negligible. An individual analysis typically consisted of 50 integrations of 8 seconds. 0.6M HNO_3 followed by a 0.6M HCl + 0.02M HF was used to flush the system between analyses. The measured $^{85}Rb/^{87}Rb$ ratio was corrected for instrumental mass fractionation (0.3–0.4%/amu) using an exponential correction and assuming $^{90}Zr/^{91}Zr = 4.5882$. On the basis of repeat analysis of rock standards, the reproducibility of Rb concentration measurements is better than 0.6%.

[19] Age corrections have been applied to the Sr and Nd isotope data assuming an age of 56 Ma for Nintoku Seamount [*Dalrymple et al.*, 1980; *Duncan and Keller*, 2004].

4. Results

[20] We divide the Site 1205 Nintoku Seamount lavas into an upper and lower alkalic series, which are separated by Unit 19B (tholeiitic basalt).

4.1. Major Elements

[21] Whole rock major element concentrations and LOI values of 33 samples of volcanic rock from Nintoku Seamount are presented in Table 2. Major element totals (total + LOI) vary from 97.05–105.38, although much of the variation is caused by 5 samples (Table 2). The major element totals of the other 28 samples are 100 ± 2 wt.%. Sample 35R-3, 108–114 from Unit 19b, which contains accumulated olivine, is the only sample that plots in the tholeiitic basalt field (Figure 3). Although alteration may increase Na_2O and K_2O contents (see Discussion), the high abundances of the more immobile elements such as TiO_2 and P_2O_5 and incompatible trace element concentrations (e.g., Nb, Zr) of the Nintoku lavas compared to Hawaiian tholeiites confirm that the former are indeed alkalic. The most evolved rock types are the conglomerate clasts from core 5R, which were not present as flow units deeper in the recovered basement section at Site 1205. The significant variation in composition of the lava clasts from the conglomerate indicate that they were derived from several discrete flow units.

[22] MgO contents vary from 1.74 to 14.9 wt.%. As MgO abundances decrease, CaO, MnO, and FeO_T (total Fe as FeO) concentrations decrease whereas P_2O_5, K_2O, Na_2O, SiO_2, Al_2O_3, and TiO_2 increase (Figures 4a–4h). The hawaiite/mugearite clasts from the conglomerate have higher TiO_2 and P_2O_5 contents than their younger counterparts from Mauna Kea, Haleakala, and Kohala volcanoes.

4.2. Trace Elements

[23] Trace element contents of the Nintoku Seamount lavas from Site 1205 are presented in Table 3. Nickel, Cr, Sc, and V generally increase down the section. One sample from Unit 19b, which contains accumulated olivine, has the highest Ni content (1135 ppm) while the hawaiites and mugearites contain the lowest concentrations of compatible trace elements. The Ni contents of the alkali basalts (<234 ppm) are too low for these lavas to represent primary melts of mantle perido-

Table 2. Major Element Abundances for Leg 197, Site 1205 Basalts[a]

ID	Depth (mbsf)	SiO_2	Al_2O_3	TiO_2	MnO	MgO	FeO*	Na_2O	K_2O	P_2O_5	CaO	Total*	LOI
5R-2, 21–25	−34.09	49.0	21.0	3.47	0.10	1.85	9.61	5.58	2.20	1.21	5.99	94.18	7.30
5R-2, 31–34	−34.19	49.6	18.1	3.01	0.13	1.80	12.5	5.09	3.61	0.91	5.33	101	3.14
5R-2, 74–77	−34.62	48.5	17.1	2.84	0.19	3.79	12.9	5.07	2.33	0.83	6.44	101	4.31
5R-2, 90–94	−34.78	47.5	17.1	2.66	0.15	5.90	14.0	4.20	0.86	0.44	7.13	98.5	3.58
5R-2, 96–100	−34.84	49.5	18.0	2.93	0.14	3.44	11.5	5.23	2.43	0.84	6.04	98.9	3.30
5R-2, 114–116	−35.02	48.6	17.5	2.96	0.13	3.04	14.1	4.84	2.12	0.84	5.87	96.0	4.22
6R-2, 8–12	−43.88	47.7	16.7	2.71	0.14	6.17	11.6	3.53	1.13	0.80	9.53	97.1	3.41
6R-2, 114–119	−45.02	48.2	17.0	2.68	0.17	6.31	10.7	3.83	1.35	0.71	9.03	97.3	3.62
10R-2, 0–5	−63.12	47.2	15.6	2.95	0.23	5.70	14.3	4.15	1.15	0.64	8.09	98.7	1.41
15R-3, 10–12	−93.65	46.9	15.7	2.47	0.20	6.84	13.8	3.37	0.73	0.43	9.59	97.8	2.50
19R-1, 80–86	−110.70	47.3	16.5	2.49	0.17	6.60	12.5	3.49	1.00	0.60	9.37	95.3	3.04
20R-5, 67–72	−125.80	47.4	15.2	2.63	0.20	5.97	13.9	3.83	0.82	0.52	9.42	96.5	1.29
21R-3, 71–76	−132.83	47.9	15.6	2.54	0.17	6.65	13.2	3.35	0.61	0.49	9.50	96.7	2.52
23R-1, 85–90	−139.75	47.8	16.1	2.61	0.19	7.02	12.7	3.44	1.08	0.49	8.60	96.6	3.27
24R-1, 51–56	−149.01	47.4	16.3	3.02	0.20	7.21	14.3	3.39	0.86	0.46	6.90	93.8	4.26
26R-2, 30–34	−169.50	47.5	15.6	2.65	0.20	6.96	13.3	3.32	0.54	0.48	9.53	96.0	3.12
27R-6, 124–129	−185.66	47.8	15.6	2.20	0.17	7.19	12.7	3.29	0.61	0.40	9.99	96.0	3.13
28R-3, 10–15	−189.75	47.5	14.8	2.19	0.20	7.17	14.0	3.21	1.01	0.34	9.57	97.0	2.22
29R-3, 18–23	−199.00	47.7	15.7	2.72	0.32	6.24	13.7	3.54	0.47	0.46	9.16	96.1	3.01
29R-4, 117–121	−201.30	48.2	16.6	2.16	0.19	6.66	12.3	3.57	0.73	0.40	9.15	96.6	4.79
32R-3, 17–22	−220.47	47.8	16.2	2.04	0.17	6.82	12.4	3.28	1.09	0.37	9.75	97.2	3.05
33R-2, 70–75	−226.61	47.6	15.7	2.38	0.19	6.74	13.1	3.23	1.07	0.43	9.60	97.6	3.26
34R-3, 79–84	−238.29	46.6	15.6	2.33	0.20	8.36	14.0	3.13	0.40	0.53	8.88	91.4	6.02
35R-3, 108–114	−247.66	46.5	12.1	1.16	0.19	16.3	13.7	1.93	0.15	0.24	7.69	91.4	7.18
36R-5, 135–139	−260.44	47.1	14.0	2.58	0.19	9.03	13.9	3.25	0.46	0.53	8.91	96.2	2.07
37R-5, 38–42	−270.02	46.8	14.9	2.84	0.19	7.37	13.9	3.36	1.11	0.71	8.86	100	1.77
38R-1, 4–7	−273.64	46.8	15.0	2.85	0.19	7.28	13.8	3.39	1.15	0.67	8.87	102	1.47
41R-3 18–23	−285.02	47.6	15.1	2.81	0.20	7.02	14.3	3.42	0.49	0.54	8.54	94.0	3.08
41R-5, 46–50	−288.24	47.5	15.5	2.70	0.22	6.57	13.9	3.37	1.05	0.50	8.72	98.0	3.10
42R-4, 12–16	−296.96	47.5	15.5	2.68	0.23	5.95	15.2	3.53	0.26	0.44	8.68	98.8	2.90
44R-2, 14–19	−313.34	47.3	16.2	3.22	0.26	5.70	14.2	3.40	0.69	0.60	8.40	93.5	5.78
44R-2, 116–121	−314.36	46.5	16.6	3.42	0.28	6.24	15.6	3.00	0.61	0.58	7.21	94.7	3.31
45R-1, 115–118	−322.65	47.1	16.3	3.19	0.21	5.35	14.3	3.56	0.93	0.59	8.47	97.5	2.21
BHVO-2 AVG		49.0	13.3	2.69	0.17	7.42	11.4	2.10	0.42	0.38	11.3		
Recommended values		49.9	13.5	2.73	0.20	7.23	12.3	2.22	0.52	0.27	11.4		
Std. Dev. (n = 15)		2.00	0.65	0.10	0.01	0.25	0.58	0.13	0.31	0.02	0.43		
BIR-1 AVG		48.9	15.9	0.99	0.18	9.96	10.9	2.10	bdl	0.08	13.7		
Recommended values		48.0	15.5	0.96	0.02	9.70	11.3	1.82	0.03	0.02	13.3		
Std. Dev. (n = 10)		3.81	1.24	0.08	0.18	0.85	0.92	0.17	0.44	0.01	1.07		
BPL-1 AVG		47.3	15.3	2.35	0.20	8.25	12.7	2.40	1.14	0.69	9.96		
Recommended values		47.3	15.3	2.40	0.20	8.30	12.5	2.40	1.10	0.50	10.0		
Std. Dev. (n = 10)		0.90	0.35	0.05	0.01	0.23	0.48	0.08	0.12	0.04	0.16		

[a] Sample data presented in this table have been normalized to 100 wt.%. bdl, below detection limit. BHVO-2 and BIR-1 recommended values from USGS preliminary certificate of analysis and USGS certificate of analysis, respectively. URLs are http://minerals.cr.usgs.gov/geo_chem_stand/basaltbhvo2.html and http://minerals.cr.usgs.gov/geo_chem_stand/icelandic.html, respectively. BPL-1 recommended values from S. Hughes, Idaho State University, personal communication. FeO*, total iron; Total*, unnormalized major element totals.

tite, indicating that they have undergone fractional crystallization within the crust. The concentration of the highly incompatible elements that are immobile during alteration (e.g., Zr, Nb) vary by a factor of ~13, with the highest concentrations in the most evolved lavas (up to 91 times primitive mantle abundances). Chondrite-normalized REE patterns of the Nintoku lavas are similar to those of similar rock types from the Hawaiian Islands (Figure 5). Hawaiites and mugearites have higher concentrations of incompatible trace elements and steeper REE patterns (La/Yb varies from 12.6–17.0) compared to the alkali basalts (La/Yb < 10.0). Ba/Th ratios (113–162) of the Nintoku lavas are high compared to most other intraplate oceanic lavas, but are similar to other Hawaiian lavas [*Yang et al.*, 2003].

4.3. Sr and Nd Isotopes

[24] Age-corrected $^{87}Sr/^{86}Sr$ ratios for the leached sample powders range from 0.703130–0.703245

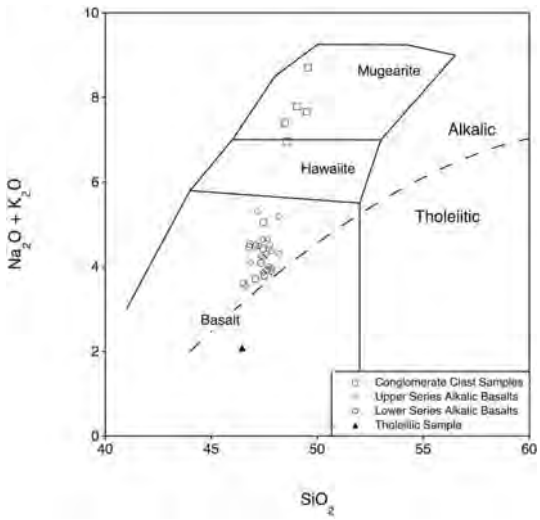

Figure 3. Classification of Site 1205 lavas, SiO_2 versus total alkalis ($Na_2O + K_2O$), where the dashed line separates Hawaiian tholeiitic and alkali lavas [*Miyashiro*, 1978]. Fields for rock types are from *Cox et al.* [1979]. All samples except for 35R-3, 108–114 are alkalic. Samples from Core 5R-2 in Unit SE II (the conglomerate overlying the volcanic basement) are predominantly more evolved than underlying alkalic basalts.

and initial $^{143}Nd/^{144}Nd$ ratios range from 0.512927–0.512990 (Table 4). Epsilon-Nd and ε_{Sr} values of the Site 1205 lavas are within the range of postshield lavas from Mauna Kea, Haleakala, and Kohala volcanoes, although ε_{Sr} is at the lower end of this range (Figure 6). One sample of alkali basalt from Site 432 analyzed by *Regelous et al.* [2003] has lower ε_{Sr} than any postshield lavas from the Hawaiian Islands. There is no systematic variation of Sr or Nd isotope composition with degree of differentiation (Figure 7). The older lavas from deeper in the borehole tend to have the highest ε_{Sr} values (Figure 8f), as discussed in the next section. ε_{Sr} correlates negatively with ratios of more to less incompatible trace elements, such as La/Yb (Figure 9).

5. Discussion

5.1. Chemical and Isotopic Variations With Depth (Stratigraphic Age) in the Site 1205 Drill Core

[25] There are significant variations in lava composition that correlate with stratigraphic position in the Site 1205 drill core. With decreasing depth (decreasing age), incompatible element concentrations and ratios of more- to less-incompatible elements (e.g., La/Yb, Nb/Zr) generally increase, and initial $^{87}Sr/^{86}Sr$ decreases (Figure 8). Epsilon-Nd shows no consistent correlation with depth. Similar compositional variations with age have been reported for the Kula postshield lavas of Haleakala volcano [*Chen et al.*, 1990], although the variation in Sr and Nd isotope ratios of the Nintoku lavas is less than half that observed in the Kula volcanics. Samples with the lowest $^{87}Sr/^{86}Sr$ values occur in the upper part of the Site 1205 drill core tend to have higher incompatible trace element contents, and have higher La/Yb and Nb/Zr ratios (Figure 9).

[26] As on Mauna Kea, and in contrast to Haleakala, alkali basalts and their differentiates (hawaiites and mugearites) are not intercalated in the postshield stage of Nintoku Seamount, but instead the more evolved rocks appear to have formed a discontinuous cap on the alkali basalts. Although the more evolved rock types are present only as clasts within the conglomerate unit immediately above basement at Site 1205, the predominance of hawaiite and mugearite compositions suggest that the stratigraphically highest lava units in this area were dominated by these rock types. The origin and petrogenetic significance of the temporal variations in lava composition are discussed further in the following sections.

5.2. Influence of Alteration on Chemistry

[27] Many of the Site 1205 lava units have undergone subaerial weathering immediately after eruption and are highly altered. Flow tops are variably weathered and oxidized, and soil horizons separate many of the flows [*Tarduno et al.*, 2002] (Figure 2). The lava flow units subsequently underwent seawater alteration after subsidence of the summit of Nintoku Seamount below sea level. Secondary alteration minerals are abundant. For example, olivine is often completely replaced by iddingsite and calcite; glass in the groundmass and in flow margins is often replaced by clay minerals. Vesicles are partially to completely filled with clay minerals, Fe-oxyhydroxides or zeolites, and calcite veins occur throughout the section. Loss on ignition (LOI) values range from 1.3 to 7.3%, reflecting the presence of secondary carbonate and water-bearing clay minerals in most of the samples, despite great care taken to sample only the freshest material. Given the abundance of secondary minerals, alteration is likely to have

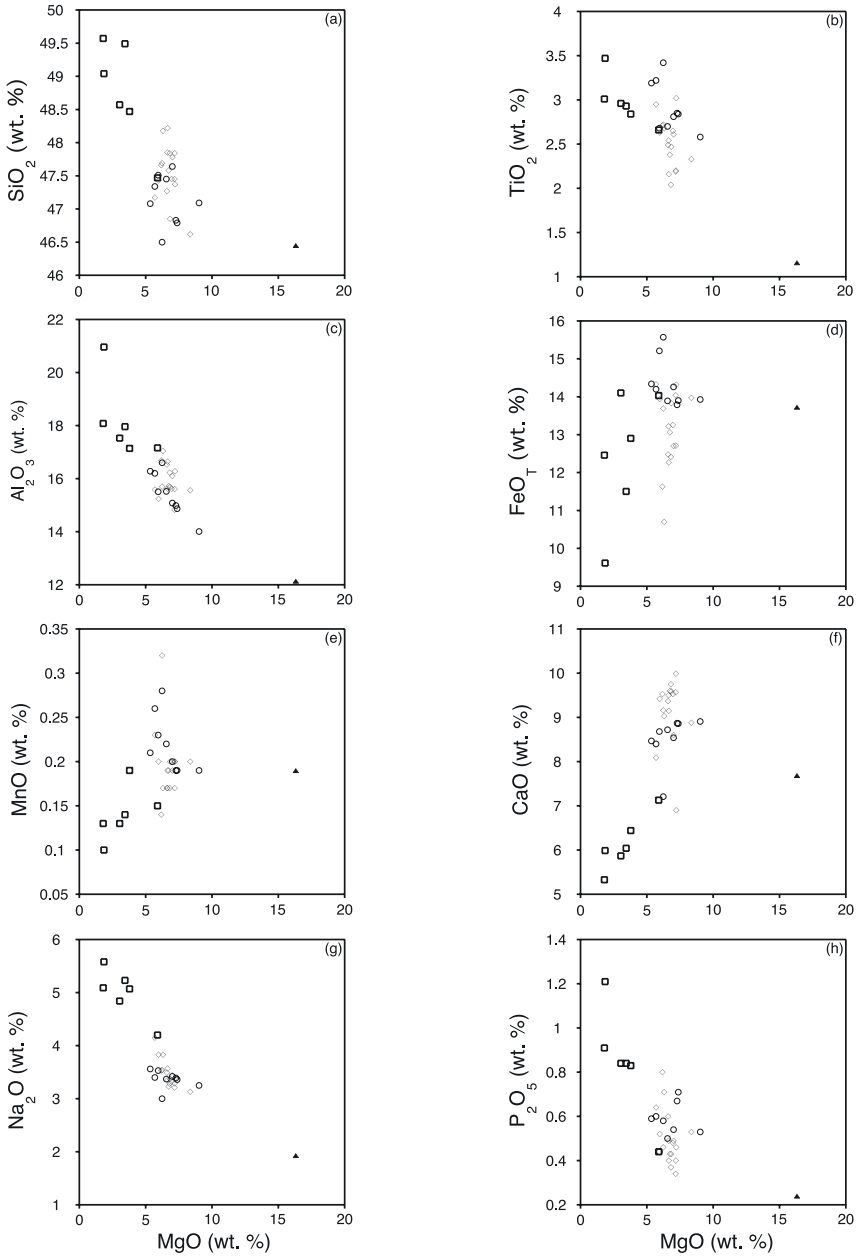

Figure 4. MgO variation diagrams. The clasts from the conglomerate form a roughly linear extension from the Core 6R-2 alkalic basalts (MgO = 6.17 and 6.31 wt.%), suggesting that they formed by fractional crystallization of melts of alkalic basalt. Symbols are the same as in Figure 3.

affected the concentrations of K, Na, and to a lesser extent, Ca, Mg, and P in the most altered samples. K_2O/P_2O_5 ratios of the Site 1205 lavas are more variable, and generally lower, than fresh postshield lavas from Haleakala (Figure 10), probably reflecting preferential loss of K during alteration [*Frey et al.*, 1994].

[28] Few of the samples analyzed have Ce/Pb, Rb/Ba, or Nb/U within range of fresh oceanic basalts (Figure 11), indicating that Pb, U, Rb, and possibly Ba were mobile during alteration. The relatively high Ce/Pb and Nb/U ratios suggest that most samples have lost U and Pb (the highest measured Nb/U ratios indicate 65% of original U content removed). Therefore, noting the influence of secondary processes on the primary chemistry of the Site 1205 lavas, we use those elements that are immobile during alteration (REE and HFSE) to investigate the petrogenesis of the Nintoku basalts

Table 3 (Representative Sample). Trace Element Abundances of Leg 197, Site 1205 Basalts[a] [The full Table 3 is available in the HTML version of this article at http://www.g-cubed.org]

ID	Li	Be	Sc	V	Cr	Co	Ni	Cu	Zn	Ga	Rb	Sr	Y	Zr	Nb	Mo	Sn	Sb	Cs	Ba	La	Ce	Pr	Nd	Sm
5R-2, 21–25	22.2	1.42	15.2	114	30.7	41.4	14.9	30.0	170	0.26	11.3	1008	36.5	276	57.4	1.20	1.69	0.35	0.20	524	43.4	82.1	11.7	44.4	9.33
5R-2, 31–34	11.4	1.83	13.9	89.3	45.8	35.5	8.32	21.7	140	12.2	30.6	907	29.0	230	57.7	2.03	1.68	0.09	0.27	617	39.6	80.0	10.2	38.2	7.63
5R-2, 74–77	14.8	1.70	13.8	98.5	44.1	28.9	9.74	23.7	175	17.0	26.7	899	26.3	233	54.5	2.20	1.37	0.18	0.22	651	36.4	67.8	9.30	35.2	7.13
5R-2, 90–94	11.7	1.16	28.2	373	194	53.6	76.4	71.3	201	29.5	13.4	432	22.1	137	25.7	1.47	1.29	0.16	0.08	233	18.2	37.8	4.99	19.1	4.45
5R-2, 96–100	17.9	1.93	14.8	100	47.0	34.9	11.1	32.1	157	13.2	48.6	920	32.3	234	64.7	3.23	1.99	0.31	0.83	659	41.5	83.5	11.0	41.1	8.33
5R-2, 114–116	16.3	1.47	14.0	85.9	50.1	37.9	9.61	19.9	149	75.0	33.3	908	27.2	217	59.8	2.98	1.51	0.13	0.43	499	30.4	60.6	8.01	29.9	6.20
6R-2, 8–12	13.3	1.59	23.6	270	140	52.9	76.5	89.6	155	49.3	19.2	728	23.5	209	40.3	1.55	6.09	bdl	0.06	383	25.4	52.9	7.10	29.2	6.28
6R-2, 114–119	14.8	1.60	23.8	267	123	60.2	76.0	62.4	164	12.8	17.1	761	21.9	166	34.9	1.70	1.11	0.12	0.11	390	28.5	59.2	7.77	29.7	6.33
10R-2, 0–5	14.0	1.67	23.2	233	147	49.2	57.7	67.4	159	44.1	22.7	547	28.5	216	42.4	2.43	8.08	0.09	0.17	392	25.5	51.5	7.04	28.5	6.58
15R-3, 10–12	9.4	1.01	29.6	367	150	56.2	76.6	97.3	153	31.2	12.4	489	23.6	132	22.6	1.24	5.25	bdl	0.08	212	15.0	33.6	4.64	19.5	4.82
19R-1, 80–86	6.61	1.24	28.3	278	105	52.2	80.2	72.6	149	35.1	17.0	773	26.1	158	30.1	1.23	6.51	0.02	0.10	281	20.2	42.5	5.95	24.2	5.77
20R-5, 67–72	9.89	1.22	27.7	311	99.5	50.4	61.2	92.0	169	27.0	18.0	560	27.1	155	28.1	1.58	6.15	0.03	0.09	246	17.7	39.1	5.36	22.8	5.70
21R-3, 71–76	12.0	1.05	29.6	351	180	56.2	78.7	83.1	151	33.1	12.9	399	24.5	146	25.4	1.17	6.05	0.03	0.11	216	14.6	31.4	4.39	18.7	4.73
23R-1, 85–90	13.3	1.16	31.2	372	174	59.1	75.4	99.7	168	37.5	14.5	399	26.4	158	27.1	1.28	6.49	0.04	0.14	225	15.8	35.5	4.81	20.1	5.02
24R-1, 51–56	19.6	1.09	37.0	440	121	63.6	68.1	107	181	37.5	15.6	421	30.6	160	27.7	1.05	6.75	0.05	0.10	239	18.3	37.8	5.44	22.8	5.66
26R-2, 30–34	6.13	1.12	28.8	363	149	52.9	93.3	92.5	159	24.8	12.7	418	24.2	143	26.1	1.15	5.59	0.02	0.04	227	16.5	36.5	5.08	21.4	5.24
27R-6, 124–129	4.93	0.89	31.7	353	246	610	112	99.3	145	28.5	9.61	360	22.6	121	18.5	1.09	5.50	0.02	0.03	157	11.1	25.2	3.60	15.5	4.05
28R-3, 10–15	6.44	0.81	33.2	363	134	60.4	74.7	103	160	28.3	6.95	341	25.3	115	17.5	1.08	4.91	0.03	0.02	142	11.6	26.1	3.77	16.3	4.29
29R-3, 18–23	4.29	1.01	29.7	379	146	50.4	66.4	76.9	162	29.1	9.18	351	27.8	152	26.2	1.42	5.80	0.03	0.03	197	16.5	37.5	5.03	21.2	5.28
29R-4, 117–121	5.39	0.74	29.1	313	241	51.8	108	89.0	146	27.4	9.15	315	22.1	112	18.3	0.95	4.60	bdl	0.02	157	12.1	27.6	3.92	16.7	4.34
32R-3, 17–22	5.06	0.89	28.1	309	186	55.2	111	88.2	132	23.9	9.95	366	21.4	112	18.1	0.91	4.50	bdl	0.04	155	12.1	28.0	3.87	15.8	4.10
33R-2, 70–75	2.66	1.05	30.6	371	206	58.8	89.5	94.6	147	33.1	11.0	395	25.9	144	25.1	1.17	5.88	0.03	0.02	218	15.4	34.1	4.70	19.4	4.68
34R-3, 79–84	4.21	1.02	25.2	257	299	65.8	185	100	144	28.9	11.5	370	26.3	160	25.4	1.10	6.13	0.05	0.05	206	16.2	35.0	4.90	20.3	4.88
35R-3, 108–114	5.09	0.67	42.3	361	1489	176	1135	135	187	24.9	1.44	335	24.2	91.1	11.4	0.73	13.2	0.05	0.02	98.7	8.10	18.5	2.74	12.3	3.61
36R-5, 135–139	14.2	1.31	25.6	298	270	65.4	234	103	179	20.9	21.9	582	22.8	136	26.9	1.38	1.21	0.02	0.04	264	20.5	40.5	5.81	22.2	5.16
37R-5, 38–42	7.25	1.53	25.6	300	173	56.9	152	103	169	28.9	18.7	632	25.7	193	34.2	1.76	6.90	0.06	0.24	313	23.7	50.8	6.89	27.2	6.19
38R-1, 4–7	6.24	1.46	26.6	336	217	63.4	149	105	171	45.0	16.2	647	25.6	199	33.7	1.89	7.14	0.04	0.13	333	22.0	47.3	6.38	26.2	5.76
41R-3 18–23	6.09	1.23	33.4	298	134	49.1	81.6	84.6	162	27.3	14.1	359	33.0	154	25.1	1.18	6.69	0.04	0.06	219	19.2	42.4	6.16	25.9	6.47
41R-5, 46–50	3.81	0.98	32.8	379	178	61.7	87.6	79.3	187	36.2	12.5	362	29.7	171	24.1	1.35	6.62	bdl	0.02	207	15.2	34.8	4.96	21.3	5.36
42R-4, 12–16	1.69	1.07	30.2	344	145	60.0	84.5	71.4	163	32.4	12.9	348	28.9	166	24.4	1.44	5.87	bdl	0.03	213	14.6	33.0	4.69	20.6	5.32
44R-2, 116–121	6.41	1.20	31.7	311	154	55.3	70.5	81.2	187	31.2	12.7	310	34.0	190	27.2	1.33	7.41	bdl	0.04	226	19.9	45.1	6.63	28.0	6.95
44R-2, 14–19	4.20	1.05	32.3	393	168	66.0	81.7	92.7	205	41.1	12.8	398	34.2	219	29.9	1.20	8.16	0.03	0.03	255	18.9	43.8	6.08	27.0	6.84
45R-1, 115–118	4.98	1.35	27.0	361	173	56.8	78.1	83.8	190	33.1	16.6	393	30.3	215	28.2	1.85	7.24	0.03	0.12	244	18.4	43.3	6.18	26.2	6.76
Recommended value	5.00	*1.10*	32.0	317	280	45.0	119	127	103	*21.7*	9.80	389	26.0	172	18.0	1.02	1.90	0.16	0.13	130	15.0	38.0	*5.70*	25.0	6.20
BHVO-2 AVG	3.86	1.03	38.0	345	351	56.2	137	151	138	25.3	10.1	407	25.8	174	19.2	3.94	5.78	0.15	0.11	142	15.5	38.4	5.72	24.8	5.99
Std. Dev. (n = 5)	1.07	0.08	2.46	47.8	46.3	3.93	10.7	18.7	19.3	2.26	0.63	19.6	0.95	16.7	0.91	1.53	3.86	0.03	0.04	6.20	0.67	0.65	0.03	0.48	0.30

[a] All values are in ppm; bdl, below detection limits. BHVO-2 recommended values from USGS preliminary certificate of analysis (http://minerals.cr.usgs.gov/geo_chem_stand/basaltbhvo2.html). Recommended values in italics are for BHVO-1 [*Govindaraju*, 1994].

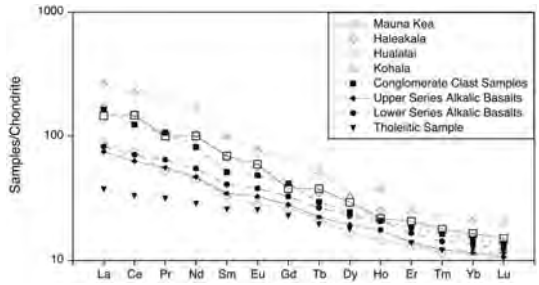

Figure 5. Chondrite-normalized REE diagram showing the average composition of the conglomerate clasts, the upper series and lower series alkalic basalts, tholeiitic sample 35R-3, 108–114, Mauna Kea, Haleakala, Hualai, and Kohala postshield basalts. The compositions of the Nintoku samples are similar to those of similar rock types from modern Hawaiian volcanoes.

[*Ludden and Thompson*, 1979; *Bienvenu et al.*, 1990].

5.3. Role of Fractional Crystallization, Crystal Accumulation, and Crustal Contamination

[29] Hawaiites and mugearites are considered to be the products of fractional crystallization of clinopyroxene-rich cumulates from alkalic magmas at depths of ~15 km [*West et al.*, 1988; *Frey et al.*, 1990; *Chen et al.*, 1991]. The major element characteristics of the hawaiite and mugearite samples from Nintoku Seamount can be modeled by using methods adapted from *Albarede* [1995]. The hawaiite/mugearite samples define a fairly linear extension in major element versus MgO variation diagrams from the alkalic basalts from Core 6R-2 (the youngest igneous basement recovered), suggesting that the evolved samples formed by fractional crystallization of a parental melt with major element characteristics similar to Core 6R-2 alkalic basalts (Figure 4). After applying a least squares fit to the major element versus MgO content of the hawaiite/mugearite and Core 6R-2 alkalic basalts, an estimate of the general parental melt was made. Using the concentrations of highly incompatible elements Nb, Th, and La from sample 5R-2, 90–94, an alkali basalt clast contained in the conglomerate with the hawaiite/mugearite samples that has major element abundances similar to the parental melt estimate, an estimate of amount of fractional crystallization was made assuming that the bulk partition coefficient, D, for these elements is approximately 0. If this is the case, then the standard Rayleigh fractional crystallization equation reduces to $C_L = C_O/F$, where C_O is

Table 4. Sr and Nd Isotope Data for Leg 197, Site 1205 Basalt

ID	Rb	Sr	$^{87}Sr/^{86}Sr$ (o)	$^{87}Sr/^{86}Sr$ (t)	ε_{Sr}	Sm	Nd	$^{143}Nd/^{144}Nd$ (o)	$^{143}Nd/^{144}Nd$ (t)	ε_{Nd}
5R-2, 21–25	11.3	1008	0.703145	0.703140	−18.4	9.33	44.4	0.512973	0.512927	7.04
5R-2, 90–94	13.4	432	0.703280	0.703220	−17.3	4.45	19.1	0.513040	0.512989	8.25
5R-2, 96–100	48.6	920	0.703192	0.703130	−18.5	8.33	41.1	0.512986	0.512941	7.32
6R-2, 8–12	19.2	735	0.703195	0.703156	−18.2	6.28	29.2	0.512995	0.512948	7.45
10R-2, 0–5	22.7	552	0.703219	0.703141	−18.4	6.58	28.5	0.513019	0.512968	7.85
15R-3, 10–12	21.1	533	0.703244	0.703174	−17.9	4.51	19.0	0.513003	0.512951	7.50
19R-1, 80–86	17.0	781	0.703247	0.703174	−17.9	6.14	24.4	0.513001	0.512946	7.41
20R-5, 67–72						6.06	23.0	0.513016	0.512958	7.67
21R-3, 71–76						4.73	18.7	0.512998	0.512942	7.34
23R-1, 85–90	14.5	404	0.703232	0.703162	−18.1	5.02	20.1	0.513025	0.512970	7.88
24R-1, 51–56	15.6	426	0.703236	0.703161	−18.1					
26R-2, 30–34	12.7	422	0.703249	0.703180	−17.8	5.57	21.6	0.513014	0.512957	7.63
27R-6, 124–129	9.61	363	0.703259	0.703199	−17.5	4.05	15.5	0.513002	0.512944	7.38
28R-3, 10–15	6.37	308	0.703246	0.703202	−17.5	4.45	16.2	0.513015	0.512954	7.58
29R-3, 18–23	9.18	355	0.703244	0.703189	−17.7					
29R-3, 92–95						5.61	21.3	0.513032	0.512974	7.96
29R-4, 117–121						4.61	16.8	0.513014	0.512954	7.56
32R-3, 17–22	15.1	349	0.703288	0.703231	−17.1	3.84	15.6	0.513011	0.512957	7.62
33R-2, 70–75	11.0	399	0.703255	0.703190	−17.7	4.68	19.4	0.513016	0.512963	7.74
34R-3, 79–84	11.5	374	0.703320	0.703236	−17.0	4.88	20.3	0.513011	0.512958	7.67
35R-3, 108–114	1.44	190	0.703208	0.703200	−17.5	2.04	7.08	0.513053	0.512990	8.26
37R-5, 38–42	18.8	638	0.703204	0.703151	−18.2	6.58	27.4	0.513020	0.512967	7.83
38R-1, 4–7	16.2	653	0.703204	0.703153	−18.2	5.76	26.2	0.513007	0.512958	7.66
41R-3, 18–23	14.1	363	0.703285	0.703200	−17.5					
42R-4, 12–16	12.9	351	0.703331	0.703245	−16.9	5.32	20.6	0.513012	0.512955	7.59
44R-2, 14–19	12.8	402	0.703299	0.703227	−17.1	6.84	27.0	0.513011	0.512955	7.59
44R-2, 116–121	21.9	309	0.703333	0.703233	−17.1	6.21	25.4	0.513005	0.512951	7.51
44R-2, 115–118						7.19	26.5	0.513003	0.512943	7.36

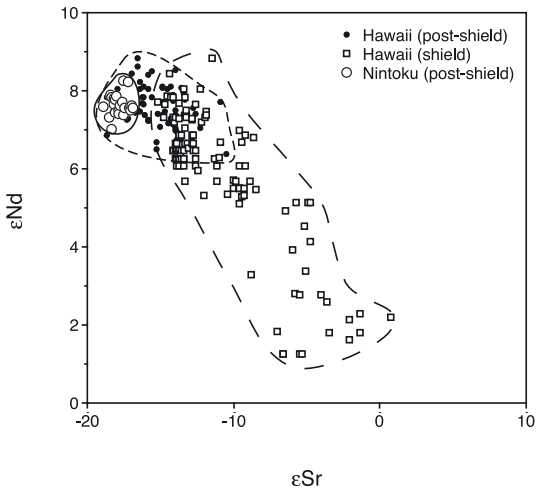

Figure 6. Plot of ε_{Sr} versus ε_{Nd} showing Hawaiian and Emperor postshield and shield basalts and the Nintoku postshield basalts. The Nintoku postshield basalts largely overlap postshield basalts from Hawaiian volcanoes, although the ε_{Sr} of the Nintoku samples extend toward the lower end of this range.

the trace element concentration of this alkali basalt clast and C_L is the average trace element concentration in the hawaiite/mugearite samples. Once an estimate of *F* is made, the major element composition of the cumulate that fractionated from the hawaiite/mugearite parental melt can also be estimated using simple mass balance approaches. Using a constrained linear least squares method presented by *Albarede* [1995], the cumulate composition was recast into proportions of mineral phases present as phenocrysts in the hawaiite/mugearite lavas. The Site 1205 lavas commonly contain olivine, plagioclase, clinopyroxene, and titanomagnetite as phenocryst phases. The theoretical cumulate composition can be represented as the vector ***y*** contained within the matrix ***A***, which has 5 columns representing the cumulate and mineral (olivine, plagioclase, clinopyroxene, and Fe-Ti oxide) compositions and 11 rows for the 11 major elements modeled. The compositions of the mineral phases were taken from electron microprobe data collected on the phenocryst phases from the Nintoku hawaiite/mugearite samples during DSDP Leg 55 [*Clague et al.*, 1980]. Manipulation of matrix ***A*** leads to the unconstrained solution, the vector ***x***. The constrained solution (the proportions of mineral phases needed to reproduce the cumulate composition) can be calculated after recalculating the unconstrained solution to force the mineral phase proportions to sum to unity. The fractional crystallization (37–58%) of a crystal assemblage composed of plagioclase, clinopyroxene, olivine, and Fe-Ti oxides in the proportions 46:30:14:10 can reproduce the trends seen in the hawaiite/mugearite samples, except for MnO (Figure 12). Model parameters are presented in Table 5.

[30] This model predicts significant plagioclase, clinopyroxene, and Fe-Ti oxide fractionation, the effects of which are only partially borne out in the trace element characteristics of the hawaiites/mugearites. Scandium is compatible in clinopyroxene [*Hart and Dunn*, 1993; *Jenner et al.*, 1993; *Green*, 1994] and the hawaiite/mugearite lavas have corresponding low Sc concentrations (<15.5 ppm) that is consistent with significant clinopyroxene fractionation. However, Sr and Eu concentrations in the hawaiite/mugearite lavas are not depleted, which is *inconsistent* with extensive fractionation of plagioclase. Certain characteristics of the Nintoku samples suggest mitigating factors. The high Sr abundances are coupled with high P_2O_5 abundances, which suggests the presence of minor mineral phases such as apatite may be controlling the Sr budget in these samples. Petrography indicates that the dominant Fe-Ti oxide species is titanomagnetite [*Tarduno et al.*, 2002] which requires relatively high oxygen fugacity conditions to crystallize (e.g., QFM). This would keep Eu in the 3+ oxidation state, thereby limiting the uptake of Eu into the fractionating plagioclase.

[31] This model can be quantitatively tested by modeling the trace element variations between the hawaiite/mugearite and the alkali basalt clasts using the mineral proportions and percent fractional crystallization derived from the major element model. Figure 13 shows that the majority of incompatible trace elements can be adequately predicted using calculated mineral proportions, except for Sr, possible reasons for which were discussed above. Modeled concentrations for all elements except Sr, Y, Yb are within 25% of measured concentrations for samples 5R-2, 21–25 and 5R-2, 96–100. For sample 5R-2, 31–34 only Sr, Y, Er, and Yb are outside this range. Samples 5R-2, 74–77 and 5R-2, 114–116 show worse agreement; the predicted HREE concentrations are systematically higher in these samples than the actual concentrations, however, increasing clinopyroxene fractionation could lower the model HREE predictions.

5.4. Role of Melting Processes and Source Heterogeneity in Creating Variation Within Nintoku Lavas

[32] Major and trace element and isotopic compositions indicate that the Nintoku lavas cannot all be

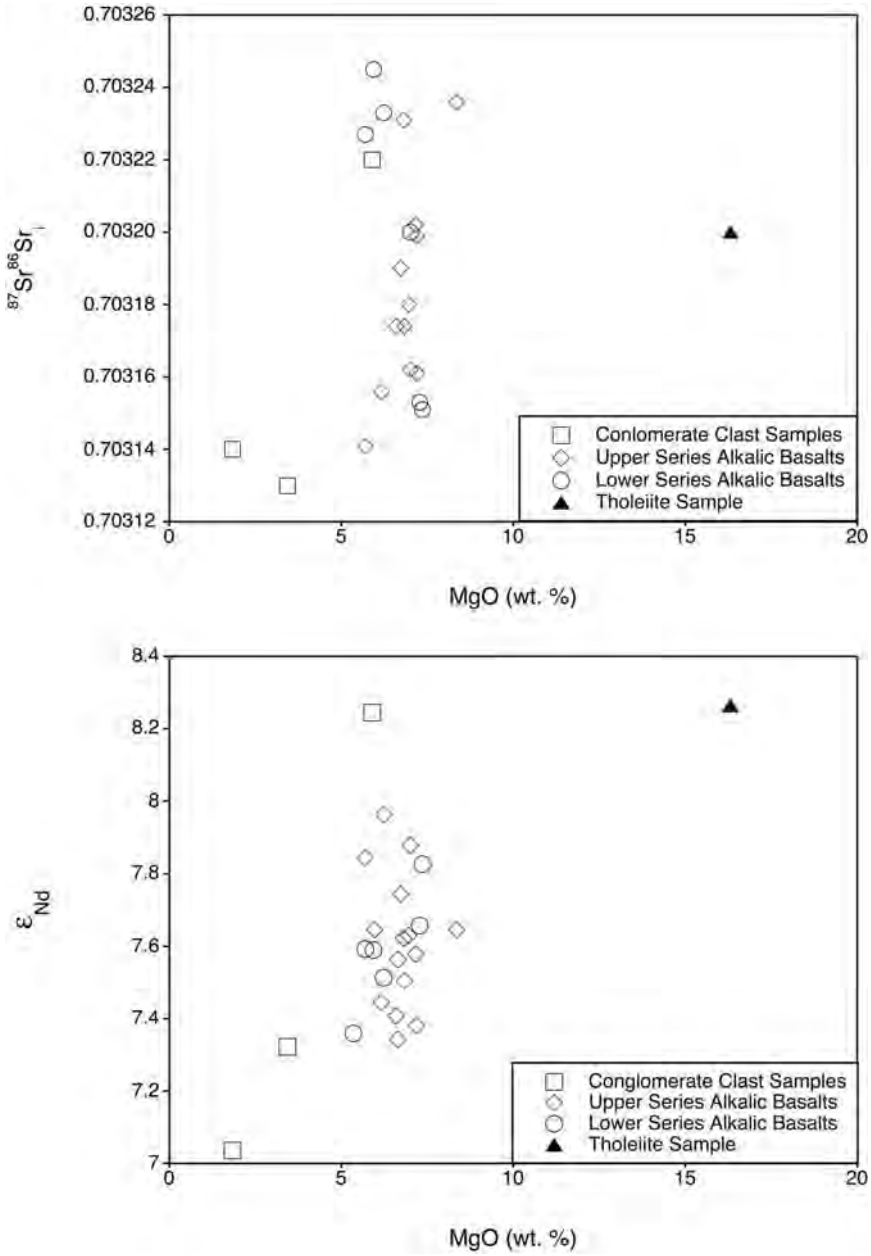

Figure 7. MgO (wt.%) versus $^{87}Sr/^{86}Sr_i$ and ε_{Nd}. Neither isotope composition varies systematically with degree of differentiation.

related simply by closed-system fractional crystallization from a single parental magma composition. At MgO contents of ~7 wt.%, there is a considerable range in SiO_2, TiO_2, FeO_T, MnO, CaO, P_2O_5, and K_2O in the alkali basalt samples (Figures 4a–4h). To some extent, these major element variations could reflect variations in the degree and pressure of melting, such that the Nintoku lavas are derived from crystallization of a range of melt compositions. However, the significant variation in Sr isotope composition, and the correlation of $^{87}Sr/^{86}Sr$ with incompatible trace element ratios (Figure 9) indicates that source heterogeneity was an important factor in creating variation with the Nintoku lavas.

[33] Mixing of two sources, or melts derived from them, followed by variable amounts of fractional crystallization could account for the trace element and isotopic variation, although the scatter in plots such as Nb/Zr versus $^{87}Sr/^{86}Sr$ requires both end-members to be heterogeneous (Figure 9). Most importantly, simple two-component mixing does not readily explain the systematic variations in

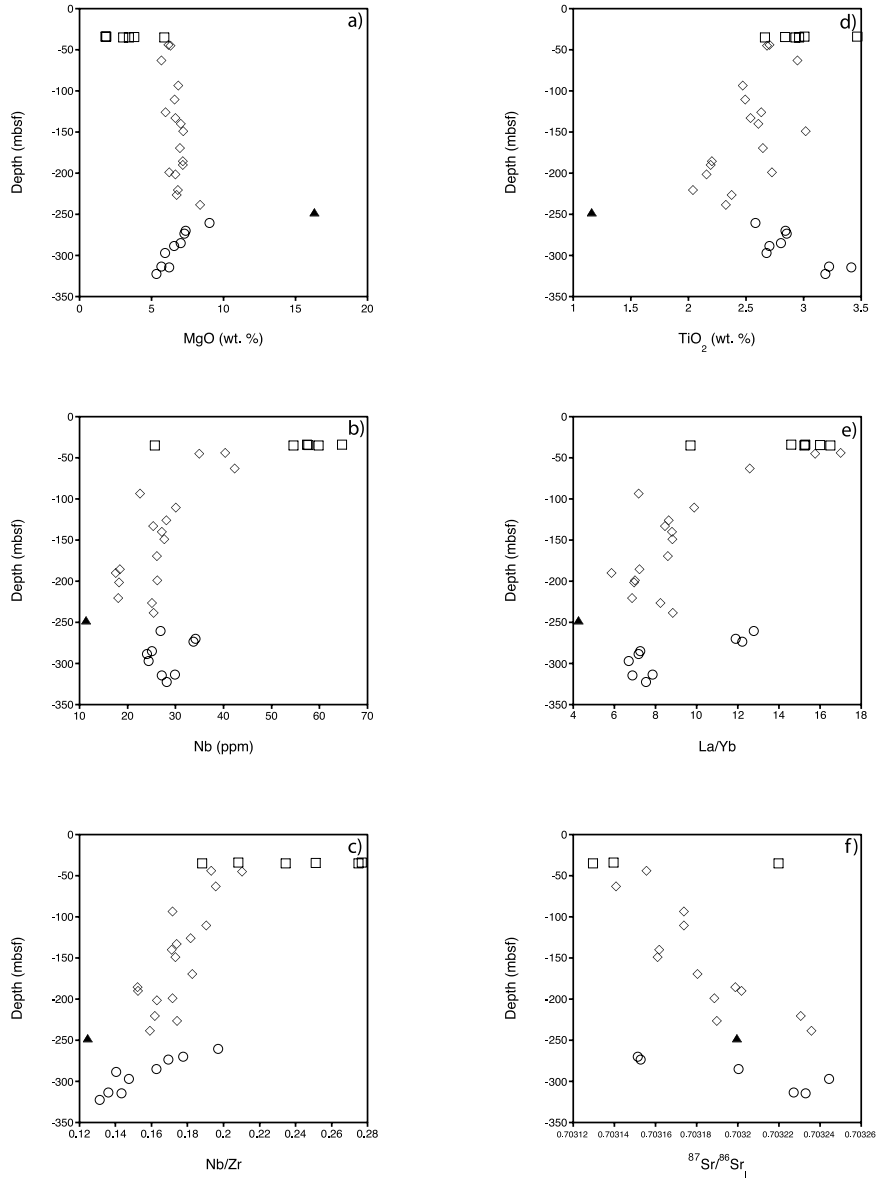

Figure 8. Depth profiles from Hole 1205A. With decreasing depth (decreasing age), incompatible element concentrations tend to increase, ratios of more- to less-incompatible elements (e.g., La/Yb, Nb/Zr) increase, and initial $^{87}Sr/^{86}Sr$ decreases.

trace element and isotopic composition with time that are observed in the lavas from Site 1205.

5.5. Model for the Formation of the Nintoku Postshield Basalts

[34] Two characteristics of the Nintoku alkali basalts must be accounted for in any model of their genesis. First, there are systematic variations in incompatible trace element and Sr isotope ratios with age: $^{87}Sr/^{86}Sr$ ratios decrease and La/Yb, Nb/Zr ratios increase with decreasing age (Figure 8). Second, lavas with the most enriched trace element compositions (highest La/Yb, Nb/Zr) were derived from a source with long-term depletion in highly incompatible elements (low $^{87}Sr/^{86}Sr$). Similar trace element-isotopic systematics characterize the transition from shield tholeiitic lavas through postshield alkali lavas to rejuvenated stage alkalic lavas of many Hawaiian volcanoes [e.g., *Chen and Frey*,

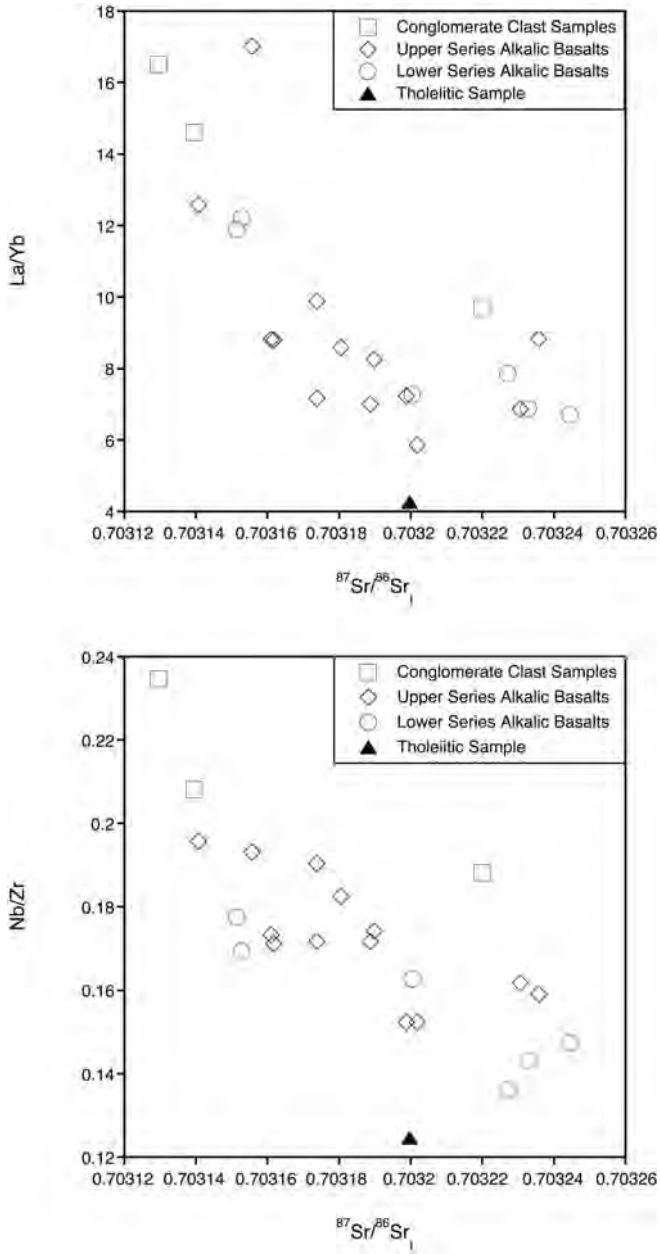

Figure 9. Initial $^{87}Sr/^{86}Sr$ versus La/Yb, Nb/Zr. Samples with the lowest $^{87}Sr/^{86}Sr_I$ tend to have higher La/Yb and Nb/Zr, suggesting a heterogeneous mantle source.

1985], and have also been recognized within the postshield alkalic lavas of Haleakala [*Chen et al.*, 1990].

[35] Several models have been proposed to account for the combination of trace element enriched lavas (high Rb/Sr, low Sm/Nd) with depleted isotope signatures (low $^{87}Sr/^{86}Sr$, high $^{143}Nd/^{144}Nd$) from Hawaii [*Chen and Frey*, 1983, 1985; *Frey and Roden*, 1987; *Reiners and Nelson*, 1998; *Yang et al.*, 2003]. Very small (<0.2%) degrees of melting of depleted mantle sources, or reactive melt transport processes are likely to result in decoupling between trace element and isotopic ratios and nonlinear variations between concentrations of incompatible elements (such as Nb and Zr), unlike those observed in Hawaiian posterosional stage lavas [e.g., *Reiners and Nelson*, 1998].

[36] Instead, many models attempting to explain the origin of Hawaiian alkali lavas invoke small-degree melts of a source that was relatively recently (<400 m.y. ago) enriched in incompatible trace elements. *Chen and Frey* [1983, 1985] proposed that partial melts of the Hawaiian plume are mixed with 1–4% of very small degree melts (0.1–1.0%)

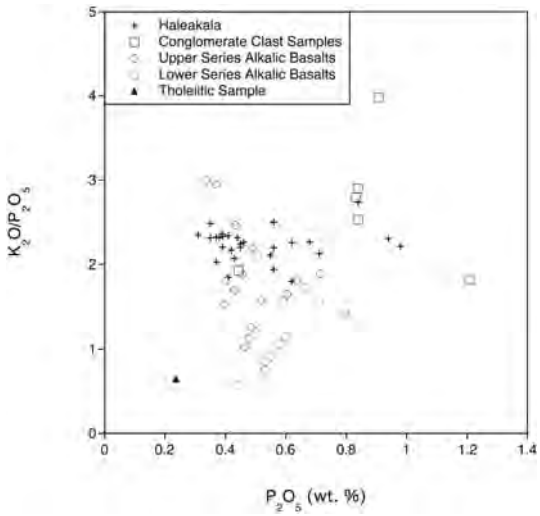

Figure 10. P_2O_5 versus K_2O/P_2O_5. The Nintoku samples tend to have lower and more variable K_2O/P_2O_5 values than Haleakala samples, reflecting preferential loss of K_2O during subaerial and submarine weathering.

of a depleted source (oceanic lithosphere or the upper mantle source of MORB). This multicomponent mixing model could account for much of the trace element and isotopic variations in lavas from Haleakala. Mixing of approximately constant proportions of the enriched source with variable-degree melts of the depleted source will result in negative correlations in La/Ce or La/Yb versus $^{87}Sr/^{86}Sr$ diagrams. A similar model, in which small-degree melts of the MORB source mantle are added to the Hawaiian plume source, and this mixed source then melted to various degrees, has been used to explain the compositions of Koloa posterosional lavas from Kauai [*Reiners and Nelson*, 1998] and the posterosional Honolulu Volcanics of Oahu [*Roden et al.*, 1994].

[37] An alternative model involves mixing of a depleted source with 0.5–2.0% of small-degree melts (~2%) from a more enriched source [*Clague and Dalyrmple*, 1988]. This is similar to metasomatic models in which small-degree partial melts of the enriched source are added to the depleted oceanic lithosphere, which subsequently undergoes partial melting to form the parental magmas of Hawaiian lavas [*Wright*, 1984]. In this model, the melt with the greatest contribution from the low $^{87}Sr/^{86}Sr$ component must have been enriched by the smallest-degree melts from the plume in order to obtain a negative correlation between $^{87}Sr/^{86}Sr$ and La/Ce or Nb/Zr. *Yang et al.* [2003] favored such a model to explain the compositions of the Honolulu Volcanics because recently determined partition coefficients imply that extremely small degree melts (<0.1%) of the depleted source would be required to explain the high La/Ce ratios of the Hawaiian posterosional lavas when using the *Chen and Frey* [1983, 1985] model. An alternative possibility, explored more fully below, is that the low $^{87}Sr/^{86}Sr$ end-member (oceanic lithosphere) is more enriched in trace elements than assumed by *Chen and Frey* [1985], perhaps by incorporation of small-degree melts of MORB source soon after its formation at the MOR axis. Below, we evaluate which of these models can best explain the trace element and isotope compositions of the Nintoku lavas.

5.5.1. Model 1: The Chen and Frey-Type Model

[38] Considering the compositional similarities between Nintoku and Haleakala postshield lavas, we first applied a multicomponent mixing model similar to that proposed by *Chen and Frey* [1985]. Distribution coefficients and model parameters are given in Table 6. Figure 14a illustrates that the Nintoku lavas can be generated by mixing of 88.4–89.2% undepleted mantle (UD) and 11.6–10.8% low-degree (0.79–1.93%) partial melts of MORB source. The amount of incipient melt mixed with UD is greater at Nintoku than for the Kula Series postshield basalts from Haleakala (97–98% UD, 2–3% MORB source), and the amount of partial melting of the MORB source required to fit the Nintoku data (0.79–1.93%) is higher than

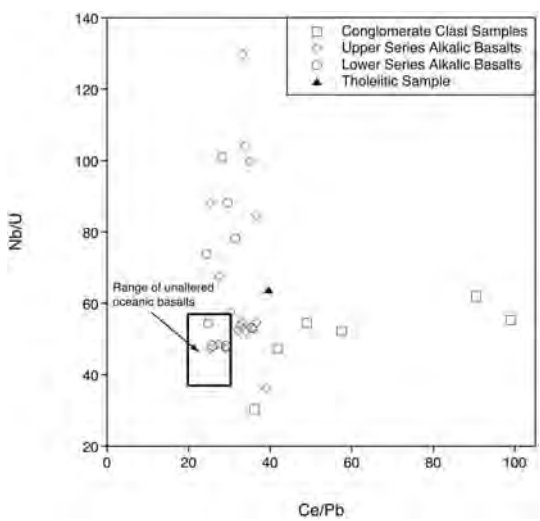

Figure 11. Ce/Pb versus Nb/U. Box shows the typical range of fresh oceanic basalts. Nintoku samples extend to higher Ce/Pb and Nb/U, suggesting that Pb and U were mobile during alteration.

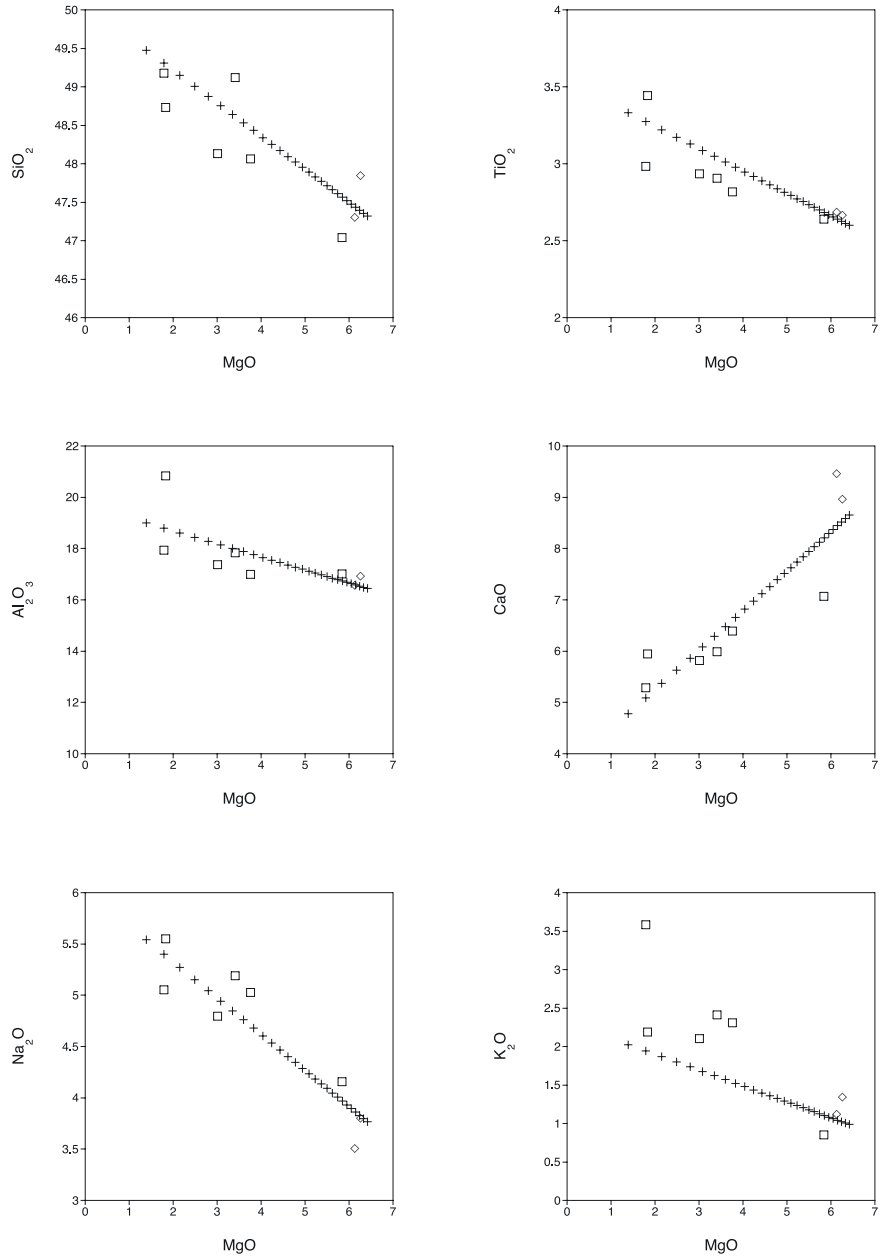

Figure 12. MgO variation diagrams showing only the conglomerate clasts and the alkalic basalts from the uppermost igneous basement. Symbols are the same as in Figure 3. The plus symbols are the hypothetical liquid line of descent if a cumulate with the composition given in Table 5 was removed from a liquid with a composition similar to the basalts from the uppermost igneous basement.

predicted for Haleakala (0.2–0.5%) [*Chen and Frey*, 1985].

[39] Following *Chen and Frey* [1985], four samples that have olivine as the only phenocryst phase were selected to quantitatively test the model. Since the model predicts only the hypothetical parental magma composition, it is necessary to correct the trace element concentrations of the selected samples for olivine fractionation in order to estimate the parental melt of each sample. Olivine addition dilutes incompatible trace element concentrations but does not radically alter trace element ratios. Equilibrium olivine was added in 1% increments until the major element composition of each sample was in equilibrium with Fo_{90} [*Chen and Frey*, 1985]. The Fe/Mg exchange coefficient between olivine and melt was 0.30 [*Ford et al.*, 1983]. This addition of olivine was then used to back-calculate the trace element

Table 5. Major Element Model Parameters[a]

	Initial	Final	Cumulate	Plag	Ol	Pyr	Ox	Cum*
SiO_2	47.3	49.1	45.8	54.1	39.5	50.0	0.0	45.6
TiO_2	2.59	3.18	2.10	0.0	0	1.67	15.3	2.00
Al_2O_3	16.4	19.0	14.3	29.0	0.15	2.77	1.43	14.4
Fe_2O_3	3.67	3.54	3.79	0.0	0.0	0.0	33.3	3.25
FeO	9.36	9.02	9.67	0.64	15.0	9.36	47.8	9.85
MnO	0.16	0.12	0.20	0.0	0.14	0.16	0.44	0.11
MgO	6.50	1.50	10.6	0.01	44.7	13.9	1.72	10.5
CaO	8.71	5.01	11.8	11.4	0.26	21.5	0..0	11.8
Na_2O	3.74	5.54	2.26	4.78	0.0	0.39	0.0	2.32
K_2O	0.97	3.01	−0.70	0.31	0.0	0.0	0.0	0.14
P_2O_5	0.60	1.03	0.26	0.0	0.0	0.0	0.0	0.0
Modal proportions				0.46	0.14	0.30	0.10	

[a] The "Initial" and "Final" compositions refer to the end-point compositions of the least squares fit of the Nintoku data presented in the MgO-variation diagrams. The "Cumulate" is the composition of the solid that needs to be removed to account for Nintoku major element variations assuming the fraction of liquid remaining at the Final compositions is 0.45 (see text for justification). This composition was recast into proportions of the four mineral phases listed above, which were then used to recalculate the cumulate composition, given as Cum* (see text for full explanation).

abundances of the parental magma assuming that olivine was the only fractionating phase. Using the corrected La abundance, we calculated how much partial melting of the hybrid UD-MORB source was required to achieve the corrected La abundance of each sample. After partially melting the hybrid source by the amount calculated above, the model results were then compared to the olivine-fractionation-corrected trace element abundances. The results are presented in Table 7.

[40] The agreement of the actual data with model predictions is generally good. In the following discussion of the model results, samples which show discrepancies of greater than or less than 25% of the actual data are considered to be in poor agreement. Predicted Rb concentrations are systematically low (21–39%) while Nb predictions are low for two of the four samples quantitatively studied (by 27% and 29% for samples 10R-2, 0–5 and 33R-2, 70–75, respectively). Thorium predictions are within 7–20% agreement and Sr predictions are within 9%, except for sample 41R-2, 18–23 (20%). Neodymium, Sm, and Hf all agree within 15%, many within 5%, of the actual data. Overall, the model adequately predicts trace element concentrations.

5.5.2. Model 2: The Yang et al.-Type Model

[41] We next applied the model of *Yang et al.* [2003] to the Nintoku data. In this model, the procedure is the basically the same as that used by *Chen and Frey* [1985], except incipient melts of Hawaiian plume source are mixed with depleted mantle lithosphere. The negative correlation between $^{87}Sr/^{86}Sr$ and La/Ce for the Nintoku data requires those samples created by the largest degree of melting to contain the smallest contribution from the low $^{87}Sr/^{86}Sr$ source (Figure 14b). Mixing proportions vary from 96.1–98.5% MORB source and 3.9–1.5% incipient melts from the Hawaiian plume (at 1.84–7.15% partial melting). Quantitative testing was performed in the same manner as above. The full results of the model are presented in Table 7. The predicted Sr, Nd, Sm, and Hf concentrations were substantially lower than those measured in the lavas (> 47% lower). Predicted Rb concentrations agreed quite well with actual data, although Rb concentrations are likely to have been affected by alteration. Thorium and Nb also show close approximation to the actual data. However, the poor reproducibility of the REE and Hf forces

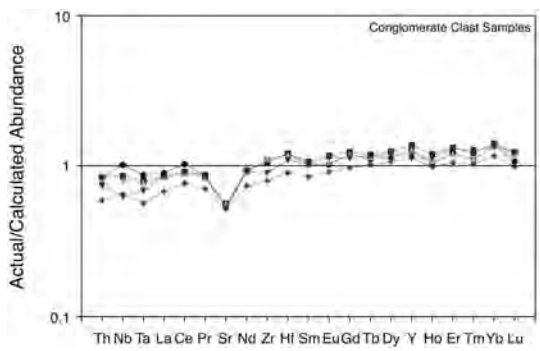

Figure 13. Major element model test figure. In this figure, the actual trace element compositions of conglomerate clasts were divided by concentrations predicted for each sample by the major element model (see text). In general, agreement between actual and predicted concentrations was good, except for Sr.

Table 6. Reservoir Compositions and Partition Coefficients[a]

	Rb	Th	Nb	Sr	Nd	Sm	Hf	La	Ce	La/Ce	$^{87}Sr/^{86}Sr$
UD	0.73	0.09	0.86	23.7	1.2	0.39	0.31	0.71	1.9	0.374	0.7047
MS	0.11	0.02	0.31	13.2	0.86	0.32	0.25	0.31	0.95	0.326	0.7023
NM	0.56	0.12	2.33	90.0	7.3	2.63	2.05	2.5	7.5	0.333	0.7023
RDS	0.61	0.14	2.51	92.2	7.42	2.64	2.06	2.66	7.73	0.345	0.7023
DML	0.041	0.005	0.11	7.0	0.49	0.31	0.17	0.11	0.34	0.326	0.7025
HP	0.85	0.11	1.4	35.9	2.2	0.69	0.53	1.4	3.4	0.407	0.7036
ol	0.003[b]	1×10^{-5}[c]	5×10^{-5}[d]	5×10^{-5}[c]	0.0003[d]	0.0009[d]	0.04[e]	0.0004[f]	0.009[g]		
cpx	0.0004[h]	0.0021[c]	0.004[i]	0.282[j]	0.35[k]	0.736[l]	0.44[m]	0.032[n]	0.057[n]		
opx	0.0002[o]	3×10^{-5}[c]	0.003[p]	0.002[p]	0.003[q]	0.03[r]	0.01[f]	0.0005[p]	0.001[p]		
gt[s]	0.0002	0.0021	0.01	0.0007	0.027	0.22	0.23	0.0164	0.065		
phl[s]	1.7		0.14	0.044	0.0063	0.0059		0.003	0.021		
amp[s]	0.023	0.001	0.08	0.27	0.23	0.32	0.3	0.075	0.11		

[a] All reservoir composition values are in ppm. UD, undepleted mantle, from *Chen and Frey* [1985]; MS, MORB source, from *Chen and Frey* [1985]; NM, normal mid-ocean ridge basalt, from *Sun and McDonough* [1989], except that $^{87}Sr/^{86}Sr$ was left the same as MORB source; RDS, refertilized depleted source, created by mixing 0.5% incipient melts of MS with NM in 0.5:99.5 proportions (see text for full description); DML, depleted mantle lithosphere, from *Yang et al.* [2003]; HP, Hawaiian plume, from *Yang et al.* [2003]. Mineral modes for calculation of the bulk partition coefficients for the model compositions above were adapted from those given by *Chen and Frey* [1985], *Halliday et al.* [1995], and *Yang et al.* [2003]. The olivine:orthopyroxene:clinopyroxene:garnet:phlogopite:amphibole proportions in the source and melt for Models 1 and 2 are as follows: Model 1, 0.6:0.25:0.1:0.05:0:0 and 0.1:0.1:0.4:0.4; Model 2, 0.55:0.25:0.15:0.05:0:0 and 0.1:0.1:0.4:0.4. Mineral proportions for MS, FDS, and melt for Model 3 are 0.706:0.2:0.05:0.02:0.002:0.02, 0.6:0.25:0.1:0.05, and 0.1:0.1:0.4:0.4, respectively. Ol, olivine; cpx, clinopyroxene; opx, orthopyroxene; gt, garnet; phl, phlogopite; amp, amphibole. Partition coefficients:
[b] *Zindler and Jagoutz* [1988],
[c] *Beattie* [1993],
[d] *Kennedy et al.* [1993],
[e] *Villemant et al.* [1981],
[f] *McKenzie and O'Nions* [1991],
[g] *Frey* [1969],
[h] *Halliday et al.* [1995],
[i] *Jenner et al.* [1993],
[j] *Sun et al.* [1974],
[k] *Skulski et al.* [1994],
[l] *Nasagawa* [1970]; *Hack et al.* [1994],
[m] *Johnson and Kinzler* [1989],
[n] *Sobolev et al.* [1996],
[o] *Kramers et al.* [1983]; *Zindler and Jagoutz* [1988]; and *Lee et al.* [1995],
[p] *Kelemen et al.* [1993],
[q] *Schwandt and McKay* [1998],
[r] *Irving and Frey* [1984],
[s] *Halliday et al.* [1995].

us to conclude that this model is not applicable to the petrogenesis of the Nintoku lavas.

5.5.3. Model 3: Modified Chen and Frey-Type Model

[42] The third model is a modified version of that proposed by *Chen and Frey* [1985]. In this model, a more enriched composition for the depleted end-member is used. Undepleted mantle is used as the enriched end-member. There is some evidence, discussed more fully in the next section, that oceanic lithosphere may be enriched by small-degree melts of MORB source soon after its formation at the ridge axis. In this model, oceanic lithosphere (N-MORB) is metasomatized by a 0.5% degree partial melt of MORB source (in 99.5:0.5% proportions, respectively) to create the "fertilized" depleted end-member. Melting of this source varies from 0.98–2.49% (as opposed to 0.79–1.93% in Model 1) and mixing proportions vary from 1.79 to 2.03% fertilized depleted end-member and 98.21 to 97.97% Hawaiian plume source (Figure 14c). The model was quantitatively tested in the same manner as the other two models and the results are presented in Table 7. Predicted trace element concentrations are significantly better than in the previous two models. Predicted Rb concentrations were all within 25% of the actual concentration (all but one sample is within 8%), which is substantially better than Model 1 and similar to the predicted concentrations from Model 2. Niobium was consistently low (> 25% for two of the four samples), which is similar to Model 1. Neodymium, Sm, Hf, and Th all agree within 16% of the actual concentration, many within 5%. The degree of incipient melting of the depleted source is higher than in Model 1 (1.78% partial melting on average versus 1.41% for Model 1) and the proportion of incipient melt mixing with Hawaiian

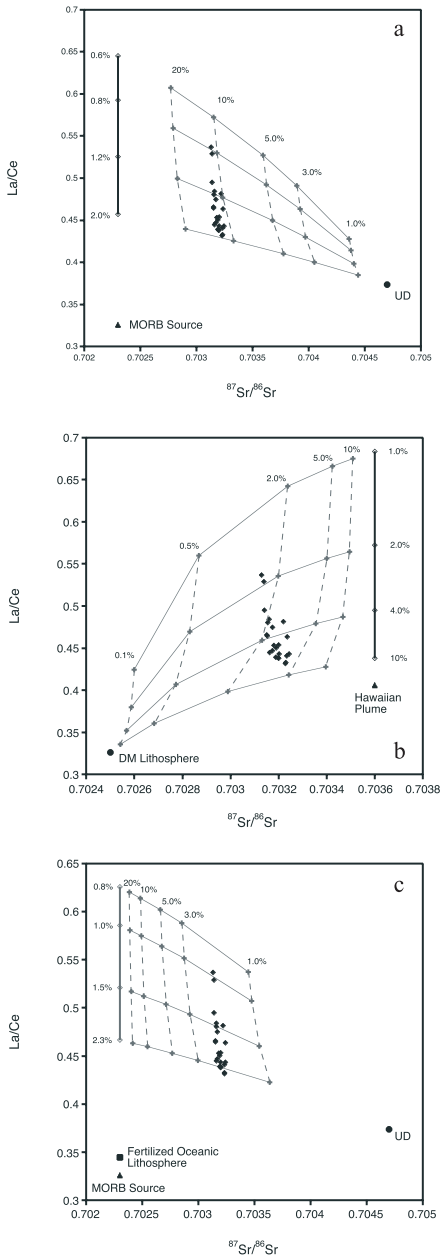

Figure 14. Plots of $^{87}Sr/^{86}Sr_I$ versus La/Ce. (a) Model 1: UD is undepleted mantle (composition is given in Table 6). Curved horizontal lines are mixing lines between incipient melts of MORB source and UD, while vertical lines are lines of equal mixing proportions. (b) Model 2: Mixing of incipient melts of Hawaiian plume (composition given in Table 6) with depleted mantle (DM) lithosphere. Notice that the trend of the data crosscuts the lines of equal mixing proportions. (c) Model 3: Mixing of incipient melts of MORB source refertilized at time of formation by small-degree melts at the mid-ocean ridge with UD. The degree of partial melting is more realistic than the extremely small degrees of melting required by Model 1.

plume source is much less than Model 1 (~2% incipient melt versus ~11% incipient melt in Model 1). As a result, smaller volumes of the oceanic lithosphere are required to melt. The amount of partial melting of the hybrid source required is also less than in Model 1 (8.55% versus 19.88% for Models 3 and 1, respectively). The results of the three models are summarized in Figure 15.

[43] The chemical and isotopic variations with time recorded in the Site 1205 lavas indicate that an increasing proportion of the incompatible trace element enriched, low $^{87}Sr/^{86}Sr$ end-member contributed to melting over the period of time represented by the Site 1205 drillcore, coupled with a lower degree of melting of this component. These temporal trends are perhaps the result of the drift of Nintoku Seamount away from the hottest part of the Hawaiian plume.

5.6. A Physical Model for Nintoku Postshield Magmatism

[44] *Chen and Frey* [1985] envisaged that Hawaiian postshield lavas were formed by melts from the Hawaiian plume mixing with incipient melts of oceanic lithosphere, which formed the wallrock of the plume conduit. The relative contribution from the radiogenic $^{87}Sr/^{86}Sr$ plume source decreased with time as the oceanic plate drifted away from the axis of the plume [*Chen and Frey*, 1985].

[45] A role for the ~90 m.y. old Pacific lithosphere in the generation of Hawaiian alkalic lavas is supported by evidence for residual phlogopite or amphibole in the source of the Honolulu Volcanics and North Arch lavas [*Clague and Frey*, 1982; *Class and Goldstein*, 1997; *Frey et al.*, 2000; *Yang et al.*, 2003]. These phases are unlikely to be stable in the convecting upper mantle, but may exist in the lower P-T conditions of the oceanic lithospheric mantle [*Class and Goldstein*, 1997]. The relatively radiogenic Os isotopic composition of many Hawaiian posterosional lavas is inferred to have been inherited from pyroxenite veins within the ~90 m.y. old Pacific oceanic lithospheric mantle beneath Hawaii [*Lassiter et al.*, 2000]. *Basu and Faggart* [1996] noted that compared to MORB, Hawaiian postshield lavas are offset to higher ε_{Sr} for a given ε_{Nd}, and suggested that they contain a seawater-altered oceanic lithosphere component.

[46] Several previous studies have argued that the lowermost parts of the oceanic lithosphere may be enriched in incompatible trace elements soon after

Table 7. Trace Element Model Results[a]

	10R-2, 0–5			33R-2, 70–75			34R-3, 79–84			41R-3, 18–23		
	Model 1[b]	Model 2[c]	Model 3[d]	Model 1[b]	Model 2[c]	Model 3[d]	Model 1[b]	Model 2[c]	Model 3[d]	Model 1[b]	Model 2[c]	Model 3[d]
f%[e]	1.10	2.75	1.37	1.61	4.99	2.04	1.38	4.37	1.74	1.56	4.85	1.97
%x[f]	11.4	1.78	1.91	11.6	2.76	2.00	10.32	3.09	1.75	11.3	2.83	1.94
F%[g]	18.9	4.97	7.53	22.1	11.1	9.77	20.2	11.2	8.83	18.4	9.41	8.07
Rb	*0.61*	0.78	0.85	0.78	0.96	1.11	0.79	0.96	1.12	0.77	0.94	1.09
Th	0.80	0.79	0.99	0.85	0.85	1.08	0.88	0.86	1.11	0.93	0.93	1.18
Nb	*0.73*	*0.74*	0.75	*0.71*	*0.72*	*0.74*	0.75	0.75	0.78	0.89	0.91	0.93
Sr	0.91	*0.56*	0.96	0.90	*0.54*	0.93	0.96	*0.60*	1.01	1.20	*0.71*	1.22
Nd	0.92	*0.58*	0.89	0.98	*0.61*	0.93	0.92	*0.59*	0.90	0.88	*0.53*	0.83
Sm	0.85	*0.60*	0.80	0.93	*0.65*	0.88	0.86	*0.61*	0.83	0.77	*0.52*	*0.71*
Hf	0.93	*0.60*	0.91	0.96	*0.61*	0.94	0.95	*0.63*	0.94	0.97	*0.61*	0.92
La[h]	1.00	1.00	1.00	1.00	1.00	1.00	1.00	1.00	1.00	1.00	1.00	1.00
Ce[h]	0.98	0.85	0.99	0.98	0.83	0.99	0.98	0.85	1.00	0.98	0.82	0.97

[a] Results are presented as the ratio of predicted abundances to actual olivine fractionation corrected abundance. Abundances that do not agree within 25% are in italics.
[b] Adaptation of model from *Chen and Frey* [1985].
[c] Adaptation of model from *Yang et al.* [2003].
[d] Adaptation of *Chen and Frey* [1985] model with enrichment of depleted source as suggested by *Halliday et al.* [1995].
[e] f%, degree of incipient melting of MORB source in C&F model, Hawaiian Plume in Yang model, and enriched MORB source in C&F-H model.
[f] %x, amount of incipient melts in the hybrid source.
[g] F%, degree of partial melting of the hybrid source.
[h] The La/Ce ratio of the samples was used to predict the melting and mixing proportions; thus the La and Ce model abundances match those of the actual samples.

formation at the ridge axis by small-degree melts of the depleted upper mantle [*Graham et al.*, 1988; *Halliday et al.*, 1995; *Lassiter et al.*, 2000]. This may then act as an important reservoir for incompatible trace elements if remobilized when later passing over a plume heat source [*Halliday et al.*, 1995; *Class and Goldstein*, 1997]. Ancient (recycled), fertilized oceanic lithosphere may represent a source for tholeiitic intraplate oceanic lavas [*Halliday et al.*, 1995; *Niu et al.*, 2002], including those from the Hawaiian hot spot [e.g., *Lassiter et al.*, 2000].

[47] We recognize that the modeling presented above is dependent on the partition coefficients, assumed end-member compositions, and modal mineral proportions of sources and crystallizing melts. These basic assumptions make the model predictions non-unique, however, the modeling does serve to show that fertilization of the oceanic lithosphere is a viable process for generating the postshield basalts of Nintoku seamount. In particular, fertilized oceanic lithosphere removes the need to invoke very small degrees of melting to account for the incompatible trace element enrichment of Hawaiian postshield and posterosional lavas. The fertilization model satisfies constraints imposed by Os isotopic compositions, which imply a significant age for the pyroxenite veins that contribute to postshield magmatism [*Lassiter et al.*, 2000] and complies with evidence for residual phlogopite/amphibole in the source of Hawaiian postshield lavas.

[48] Recently, *Frey et al.* [2005] have suggested that the depleted (low $^{87}Sr/^{86}Sr$) component in both the oldest Emperor Seamount lavas, and younger Hawaiian post erosional lavas is the same, and that it is intrinsic to the Hawaiian plume and distinct from the source of MORB. This model has some difficulty in explaining the incompatible trace element enriched compositions of Hawaiian post shield alkalic lavas, although it is possible that heat consumed by melting of the high $^{87}Sr/^{86}Sr$ "veins" inhibits melting of the more refractory matrix until the "veins" are exhausted, at which point they are more depleted in incompatible trace elements than the matrix.

5.7. Constraints From Sr Isotope Variations With Time on Petrogenesis of Hawaiian-Emperor Postshield Lavas

[49] Previous studies have shown that ε_{Sr} values of tholeiitic lavas decrease northward along the Emperor Seamount Chain (Figure 16a). The origin of the depleted isotopic compositions of the older Emperor tholeiites is debated, but likely reflects the fact that the oldest Emperor Seamounts were formed close to a former spreading center (Figure 16b). The major and trace element compositions of Detroit Seamount lavas, which indicate that they

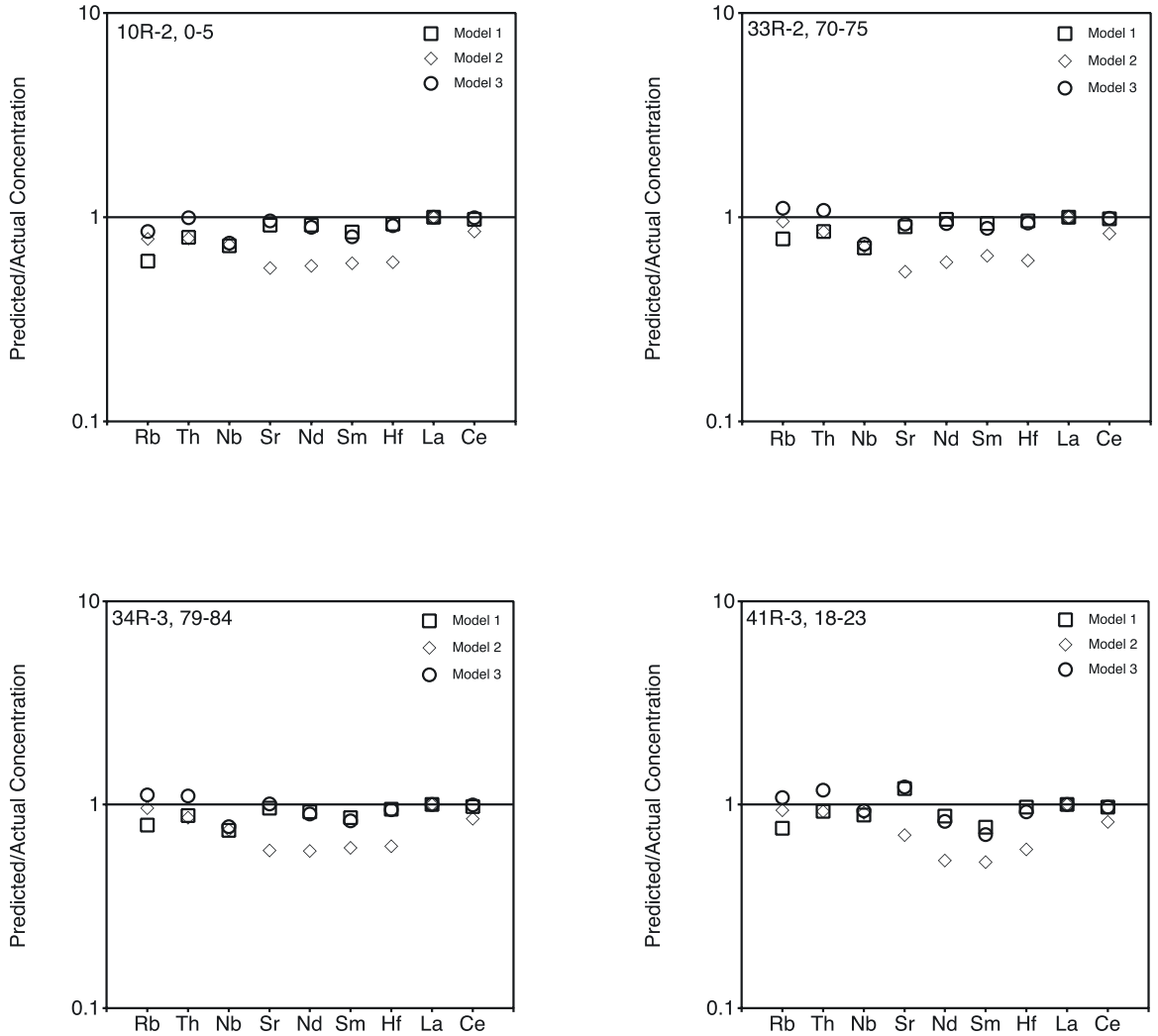

Figure 15. Graphical representation of the results of the three models presented in Figure 14. Overall, Model 3 more accurately predicts the concentrations of the elements modeled.

were derived by larger degrees of melting at lower average pressure than young Hawaiian lavas [*Huang et al.*, 2005]. *Keller et al.* [2000] suggest that the depleted compositions of older Emperor lavas are the result of plume-ridge interaction, such that the Hawaiian plume entrained depleted upper mantle and young, hot lithosphere. Alternatively, the depleted compositions of these lavas may result from melting of a depleted, refractory mantle component that contributes to melting only when the Hawaiian plume is situated beneath young, thin lithosphere where decompression melting extended to shallower depths [*Regelous et al.*, 2003; *Frey et al.*, 2005; *Huang et al.*, 2005]

[50] Together with other Leg 197 data [*Huang et al.*, 2005], our new results show that ε_{Sr} values of postshield lavas also decrease northward along the ESC (Figure 16a). Alkalic lavas from ODP Sites 883 and 1204 on Detroit Seamount, which are considered to represent postshield lavas [*Huang et al.*, 2005] have lower ε_{Sr} than any postshield or posterosional lavas reported from the Hawaiian Islands. Two samples of alkali basalt from Suiko Seamount have ε_{Sr} values that are intermediate between those of postshield alkalic lavas from the Hawaiian Islands and from Detroit Seamount [*Lanphere et al.*, 1980]. ε_{Sr} values of most Nintoku lavas are within the range of Hawaiian postshield lavas, but lie at the depleted end of this range (Figures 6 and 16).

[51] The lower ε_{Sr} values of older Emperor postshield lavas could reflect the fact that ε_{Sr} values of the plume-derived end-member was lower when the Hawaiian plume was situated close to a ridge axis, so that plume-lithosphere melt mixtures from which the alkali basalts were derived also had less radiogenic

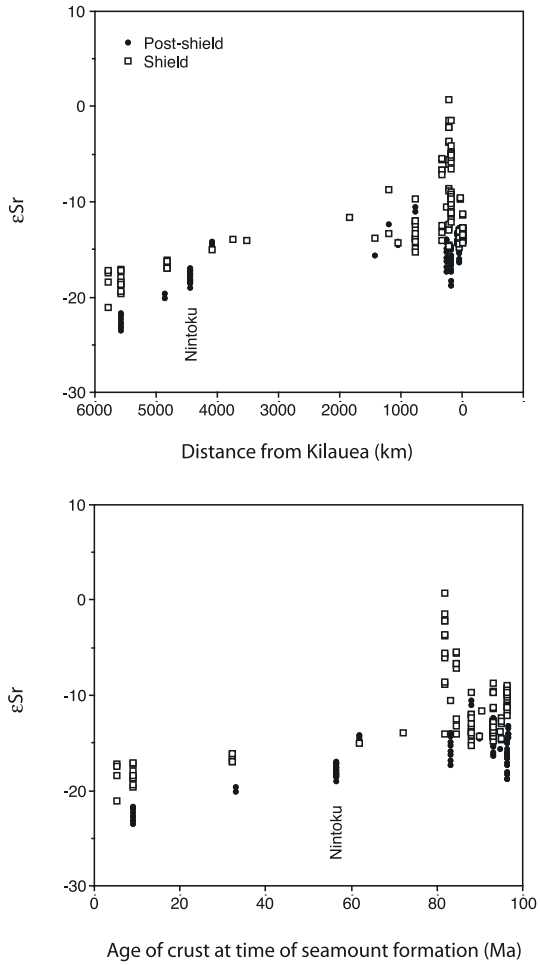

Figure 16. Distance from Kilauea (km) versus ε_{Sr} and age of crust at time of seamount formation versus ε_{Sr}. Shield and postshield data for Hawaiian volcanoes and ESC seamounts are from the GEOROC database.

Sr. However, in this case, tholeiitic lavas would be expected to have a greater range in ε_{Sr}, and to show a more pronounced decrease in ε_{Sr} with distance northward along the ESC. The available data suggest that this is not the case (Figure 16). We can rule out the possibility that postshield lavas from the older Emperor Seamounts contain a larger contribution from the low $^{87}Sr/^{86}Sr$, incompatible trace element enriched, lithospheric end-member, because this does not explain the low incompatible trace element concentrations and low La/Ce, Nb/Zr in alkalic lavas from Detroit, compared to young Hawaiian postshield lavas. Similarly, ingrowth of ^{87}Sr in old, metasomatized lithosphere with high Rb/Sr does not explain the low incompatible element concentrations of the Detroit lavas.

[52] One possible explanation for the observed temporal variation in ε_{Sr} of postshield lavas is that younger oceanic lithosphere has lower incompatible trace element concentrations and lower $^{87}Sr/^{86}Sr$. If the oceanic lithosphere is fertilized over periods of several tens of m.y. [*Niu et al.*, 2002; *Niu and O'Hara*, 2003], by small-degree melts with higher $^{87}Sr/^{86}Sr$ than normal depleted upper mantle, then the $^{87}Sr/^{86}Sr$ and incompatible trace element content of the bulk oceanic lithosphere will increase with time, and postshield lavas from seamounts formed on older crust will inherit higher ε_{Sr} and La/Ce.

[53] Alternatively, a higher degree of melting of the low $^{87}Sr/^{86}Sr$, lithospheric end-member might also explain the lower ε_{Sr}, La/Ce and incompatible trace element concentrations of the older Emperor postshield lavas, if more depleted components, with lower $^{87}Sr/^{86}Sr$, have higher melting temperatures. Increased decompression melting might be expected in the lower portions of young, thin oceanic lithosphere which would be uplifted to a greater extent above the Hawaiian plume. These two hypotheses could perhaps be tested by comparing volumes of postshield stage lavas along the ESC, although we note that postshield lava volumes on the Hawaiian Islands are highly variable.

6. Conclusions

[54] 1. Alkali basalts and their differentiates from Nintoku Seamount have similar major and trace element compositions to lavas from the postshield stage of young volcanoes from the Hawaiian Islands. Least squares modeling indicates that fractional crystallization of olivine, plagioclase, clinopyroxene, and Fe-Ti oxides can account for much of the chemical variation within the lava sequence.

[55] 2. A modified version of the *Chen and Frey* [1985] model for the origin of Hawaiian postshield lavas, in which melts of the Pacific oceanic lithosphere, previously metasomatized by small-degree upper mantle melts, are mixed with melts of Hawaiian plume mantle is proposed to explain the incompatible trace element and isotopic compositions of the Nintoku lavas, without the need to invoke very small degrees of melting.

[56] 3. Sr and Nd isotope compositions of postshield lavas from Nintoku Seamount are within the range of postshield lavas from the Hawaiian Islands, but lie at the depleted end of this range. ε_{Sr} values of postshield, as well as shield lavas decrease northward along the Emperor Seamount Chain. This could reflect either (a) increased melting of the low $^{87}Sr/^{86}Sr$ end-member beneath

volcanoes situated on younger oceanic lithosphere, or (b) less incompatible trace element enrichment (metasomatism) in the lower portions of younger oceanic lithosphere.

Acknowledgments

[57] We are deeply indebted to the officers and crew of the R.V. *JOIDES Resolution* for the help and professionalism in obtaining drill cores during ODP Leg 197. We would like to thank Dennis Birdsell and the Center for Environmental Science and Technology (CEST) at the University of Notre Dame for help with ICP-OES analysis. We thank Adam Kent and associate editor Bob Duncan for reviews. M.R. gratefully acknowledges a grant from the Deutsche Forchungsgemeinschaft while at Mainz. This research used samples provided by the Ocean Drilling Program (ODP), which is sponsored by the U.S. National Science Foundation and participating countries under management of the Joint Oceanographic Institutions Inc. Funding for the research was provided by grants form the United States Science Support Program to C. R. Neal.

References

Albarede, F. (1995), *Introduction to Geochemical Modeling*, pp. 278–282, Univ. of Cambridge Press, New York.

Basu, A. R., and B. E. Faggart (1996), Temporal isotopic variations in the Hawaiian mantle plume: The Lanai anomaly, the Molokai fracture zone and a seawater-altered lithospheric component in Hawaiian volcanism, in *Earth Processes: Reading the Isotopic Code*, *Geophys. Monogr. Ser.*, vol. 95, edited by A. R. Basu and S. Hast, pp. 149–159, AGU, Washington, D. C.

Beattie, P. (1993), The generation of uranium series disequilibria by partial melting of spinel peridotite: Constraints from partitioning studies, *Earth Planet. Sci. Lett.*, *117*, 379–391.

Bence, A. E., S. R. Taylor, and M. R. Fisk (1980), Major- and trace-element geochemistry of basalts from Ojin, Nintoku, and Suiko Seamounts of the Emperor Seamount Chain: DSDP-IPOD Leg 55, *Initial Rep. Deep Sea Drill. Proj.*, *55*, 599–605.

Bienvenu, P., J. Bougault, J. L. Joron, M. Treuil, and L. Dmitriev (1990), MORB alteration: Rare-earth element/non-rare-earth hygromagmaphile element fractionation, *Chem. Geol.*, *82*, 1–14.

Chen, C. Y., and F. A. Frey (1983), Origin of Hawaiian tholeiite and alkalic basalt, *Nature*, *302*, 785–789.

Chen, C. Y., and F. A. Frey (1985), Trace element and isotopic geochemistry of lavas from Haleakala volcano, east Maui, Hawaii: Implications for the origin of Hawaiian basalts, *J. Geophys. Res.*, *90*(B10), 8743–8768.

Chen, C. Y., F. A. Frey, and M. O. Garcia (1990), Evolution of alkalic lavas at Haleakala Volcano, East Maui, Hawaii: Major, trace element and isotopic constraints, *Contrib. Mineral. Petrol.*, *105*(2), 197–218.

Chen, C. Y., F. A. Frey, M. O. Garcia, G. B. Dalyrmple, and R. Hart (1991), The tholeiite to alkalic basalt transition at Haleakala Volcano, Maui, Hawaii, *Contrib. Mineral. Petrol.*, *106*, 183–200.

Clague, D. A., and M. H. Beeson (1980), Trace element geochemistry of the East Molokai Volcanic Series, Hawaii, *Am. J. Sci.*, *280-A*, 820–844.

Clague, D. A., and G. B. Dalyrmple (1973), Age of Koko Seamount, Emperor Seamount Chain, *Earth Planet. Sci. Lett.*, *17*, 411–415.

Clague, D. A., and G. B. Dalyrmple (1988), Age and petrology of alkalic postshield and rejuvenated-stage lava from Kauai, Hawaii, *Contrib. Mineral. Petrol.*, *99*(2), 202–218.

Clague, D. A., and F. A. Frey (1980), Trace-element geochemistry of tholeiitic basalts from Site 433C, Suiko Seamount, *Initial Rep. Deep Sea Drill. Proj.*, *55*, 559–569.

Clague, D. A., and F. A. Frey (1982), Petrology and trace element geochemistry of the Honolulu Volcanics, Oahu: Implications for the oceanic mantle below Hawaii, *J. Petrol.*, *23*(3), 447–504.

Clague, D. A., M. R. Fisk, and A. E. Bence (1980), Mineral chemistry of basalts from Ojin, Nintoku, and Suiko Seamounts, Leg 55 DSDP, *Initial Rep. Deep Sea Drill. Proj.*, *55*, 607–638.

Class, C., and S. L. Goldstein (1997), Plume-lithosphere interactions in the ocean basins: Constraints from the source mineralogy, *Earth Planet. Sci. Lett.*, *150*, 245–260.

Cox, K. G., J. D. Bell, and R. J. Pankhurst (1979), *The Interpretation of Igneous Rocks*, Allen and Unwin, St Leonards, NSW, Australia.

Dalrymple, G. B., and D. A. Clague (1976), Age of the Hawaiian-Emperor bend, *Earth Planet. Sci. Lett.*, *31*, 313–329.

Dalrymple, G. B., and M. O. Garcia (1980), Age and chemistry of volcanic rocks dredged from Jingu Seamount, Emperor Seamount Chain, *Initial Rep. Deep Sea Drill. Proj.*, *55*, 685–693.

Dalrymple, G. B., M. A. Lanphere, and D. A. Clague (1980), Conventional and $^{40}Ar/^{39}Ar$ K-Ar ages of volcanic rocks from Ojin (Site 430), Nintoku (Site 432), and Suiko (site 433) seamounts and the chronology of volcanic propagation along the Hawaiian-Emperor chain, *Initial Rep. Deep Sea Drill. Proj.*, *55*, 659–676.

Duncan, R. A., and R. A. Keller (2004), Radiometric ages for basement rocks from the Emperor Seamounts, ODP Leg 197, *Geochem. Geophys. Geosyst.*, *5*, Q08L03, doi:10.1029/2004GC000704.

Engel, A. E. J., C. G. Engel, and R. G. Havens (1965), Chemical characteristics of oceanic basalts and the upper mantle, *Geol. Soc. Am. Bull.*, *76*(7), 719–734.

Ford, C. E., D. G. Russell, J. A. Cravin, and M. R. Fisk (1983), Olivine liquid equilibria: Temperature, pressure and composition dependence of the crystal/liquid cation partition coefficients for Mg, Fe^{2+}, Ca and Mn, *J. Petrol.*, *24*, 256–265.

Frey, F. A. (1969), Rare earth abundances in a high-temperature peridotite intrusion, *Geochim. Cosmochim. Acta*, *33*(11), 1429–1447.

Frey, F. A., and M. F. Roden (1987), The mantle source for the Hawaiian Islands: Constraints from the lavas and ultramafic inclusions, in *Mantle Metasomatism*, edited by M. Menzies, pp. 423–463, Elsevier, New York.

Frey, F. A., W. S. Wise, M. O. Garcia, H. B. West, S. T. Kwon, and A. K. Kennedy (1990), Evolution of Mauna Kea Volcano, Hawaii: Petrologic and geochemical constraints on postshield volcanism, *J. Geophys. Res.*, *95*(2), 1271–1300.

Frey, F. A., M. O. Garcia, and M. F. Roden (1994), Geochemical characteristics of Koolau Volcano: Implications of intershield geochemical differences among Hawaiian volcanoes, *Geochim. Cosmochim. Acta*, *58*(5), 1441–1462.

Frey, F. A., D. Clague, J. J. Mahoney, and J. M. Sinton (2000), Volcanism at the edge of the Hawaiian Plume: Petrogenesis of submarine alkalic lavas from the North Arch Volcanic Field, *J. Petrol.*, *41*(5), 667–691.

Frey, F. A., S. Huang, J. Blichert-Toft, M. Regelous, and M. Boyet (2005), Origin of depleted components in basalt related to the Hawaiian hot spot: Evidence from isotopic and incompatible element ratios, *Geochem. Geophys. Geosyst.*, *6*, Q02L07, doi:10.1029/2004GC000757.

Govindaraju, K. (1994), 1994 compilation of working values and sample description for 383 geostandards, *Geostand. Newsl.*, *18*, 1–158.

Graham, D. W., A. Zindler, M. Kurz, W. J. Jenkins, R. Batiza, and H. Staudigel (1988), He, Pb, Sr and Nd isotope constraints on magma genesis and mantle heterogeneity beneath young Pacific seamounts, *Contrib. Mineral. Petrol.*, *99*(4), 446–463.

Green, T. H. (1994), Experimental studies of trace-element partitioning applicable to igneous petrogenesis—Sedona 16 years later, *Chem. Geol.*, *117*, 1–36.

Hack, P. J., R. L. Nielsen, and A. D. Johnston (1994), Experimentally determined rare-Earth element and Y partitioning behavior between clinopyroxene and basaltic liquids at pressures up to 20 kbar, *Chem. Geol.*, *117*, 89–105.

Halliday, A. N., D. C. Lee, S. Tommasini, G. R. Davies, C. R. Paslick, J. G. Fitton, and D. E. James (1995), Incompatible trace elements in OIB and MORB and source enrichment in the sub-oceanic mantle, *Earth Planet. Sci. Lett.*, *133*, 379–395.

Hart, S. R., and T. Dunn (1993), Experimental cpx/melt partitioning on melting of garnet peridotite, *Nature*, *363*, 63–65.

Huang, S., M. Regelous, T. Thordarson, and F. A. Frey (2005), Petrogenesis of lavas from Detroit Seamount: Geochemical differences between Emperor Chain and Hawaiian volcanoes, *Geochem. Geophys. Geosyst.*, *6*, Q01L06, doi:10.1029/2004GC000756.

Irving, A. J., and F. A. Frey (1984), Trace-element abundances in megacrysts and their host basalts—Constraints on partition coefficients and megacryst genesis, *Geochim. Cosmochim. Acta*, *48*(6), 1201–1221.

Ito, G., and J. J. Mahoney (2005a), Flow and melting of a heterogeneous mantle: 1. Method and importance to the geochemistry of ocean island and mid-ocean ridge basalts, *Earth Planet. Sci. Lett.*, *230*, 29–46.

Ito, G., and J. J. Mahoney (2005b), Flow and melting of a heterogeneous mantle: 2. Implications for a chemically non-layered mantle, *Earth Planet. Sci. Lett.*, *230*, 47–63.

Jenner, G. A., S. F. Foley, S. E. Jackson, T. H. Green, B. J. Fryer, and H. P. Longerich (1993), Determination of partition coefficients for trace elements in high pressure-temperature experimental run products by laser ablation microprobe-inductively coupled plasma-mass spectrometry (LAM-ICP-MS), *Geochim. Cosmochim. Acta*, *57*(23–24), 5099–5103.

Johnson, K. T. M., and R. J. Kinzler (1989), Partitioning of REE, Ti, Zr, Hf, and Nb between clinopyroxene and basaltic liquid: An ion microprobe study, *Eos Trans. AGU*, *70*, 1388.

Kelemen, P. B., N. Shimizu, and T. Dunn (1993), Relative depletion of niobium in some arc magmas and the continental crust: Partitioning of K, Nb, La, and Ce during melt/rock reaction in the upper mantle, *Earth Planet. Sci. Lett.*, *120*, 111–134.

Keller, R. A., R. A. Duncan, and M. R. Fisk (1995), Geochemistry and $^{40}Ar/^{39}Ar$ geochronology of basalts from ODP Leg 145 (North Pacific Transect), *Proc. Ocean Drill. Program Sci. Results*, *145*, 333–345.

Keller, R. A., M. R. Fisk, and W. M. White (2000), Isotopic evidence for Late Cretaceous plume-ridge interaction at the Hawaiian hotspot, *Nature*, *405*, 673–676.

Kennedy, A. K., G. E. Lofgren, and G. J. Wasserburg (1993), An experimental study of trace element partitioning between olivine, orthopyroxene, and melt in chondrules: Equilibrium values and kinetic effects, *Earth Planet. Sci. Lett.*, *115*, 177–195.

Kinman, W. S., and C. R. Neal (2002), The influence of MORB on a plume-generated seamount: The story told by plagioclase phenocrysts from Detroit Seamount Lavas, Emperor Seamount Chain, *Eos Trans. AGU*, *83*(47), Fall Meet. Suppl., Abstract T61C.

Kirkpatrick, R. J., D. A. Clague, and W. Freisen (1980), Petrology and geochemistry of volcanic rocks, DSDP Leg 55, Emperor Seamount Chain, *Initial Rep. Deep Sea Drill. Proj.*, *55*, 509–557.

Kramers, J. D., J. C. M. Roddick, and J. B. Dawson (1983), Trace element and isotopic studies on veined, metasomatic, and 'MARID' xenoliths from Bultfontein, South Africa, *Earth Planet. Sci. Lett.*, *65*, 90–106.

Lanphere, M. A., and F. A. Frey (1987), Geochemical evolution of Kohala Volcano, Hawaii, *Contrib. Mineral. Petrol.*, *95*(1), 100–113.

Lanphere, M. A., G. B. Dalrymple, and D. A. Clague (1980), Rb-Sr sytematics of basalts from the Hawaiian-Emperor Volcanic Chain, *Initial Rep. Deep Sea Drill. Proj.*, *55*, 695–706.

Lassiter, J. C., E. H. Hauri, P. W. Reiners, and M. O. Garcia (2000), Generation of Hawaiian post-erosional lavas by melting of a mixed lherzolite/pyroxenite source, *Earth Planet. Sci. Lett.*, *178*, 269–284.

Lee, D. C., A. N. Halliday, G. Davies, E. J. Essene, J. G. Fitton, and R. Temdjim (1995), Melt enrichment of shallow depleted mantle: A detailed petrological, trace element, and isotopic study of mantle derived xenoliths and megacrysts from the Cameroon line, *J. Petrol.*, *37*, 415–441.

Ludden, J., and G. Thompson (1979), An evaluation of the behavior of the rare earth elements during the weathering of sea-floor basalt, *Earth Planet. Sci. Lett.*, *43*, 85–92.

Macdonald, G. A., and T. Katsura (1964), Chemical compositions of Hawaiian lavas, *J. Petrol.*, *5*(1), 82–133.

Mammerickx, J., and G. F. Sharman (1988), Tectonic evolution of the North Pacific during the Cretaceous Quiet Period, *J. Geophys. Res.*, *93*, 3009–3024.

McKenzie, D., and R. K. O'Nions (1991), Partial Melt Distributions from Inversion of Rare Earth Element Concentrations, *J. Petrol.*, *12*(5), 1031–1091.

Miyashiro, A. (1978), Nature of alkalic volcanic rock series, *Contrib. Mineral. Petrol.*, *66*(1), 91–104.

Nasagawa, H. (1970), Rare Earth concentrations in zircon and apatite and their dacite and granites, *Earth Planet. Sci. Lett.*, *9*, 359–364.

Neal, C. R. (2001), Interior of the Moon: The presence of garnet in the primitive deep lunar mantle, *J. Geophys. Res.*, *106*(E11), 27,865–27,885.

Niu, Y., and M. J. O'Hara (2003), Origin of ocean island basalts: A new perspective from petrology, geochemistry, and mineral physics considerations, *J. Geophys. Res.*, *108*(B4), 2209, doi:10.1029/2002JB002048.

Niu, Y., M. Regelous, I. J. Wendt, R. Batiza, and M. J. O'Hara (2002), Geochemistry of near-EPR seamount: importance of source vs. process and the origin of enriched mantle component, *Earth Planet. Sci. Lett.*, *199*, 327–345.

Powers, H. A. (1955), Composition and origin of basaltic magma of the Hawaiian Islands, *Geochim. Cosmochim. Acta*, *7*(1–2), 77–107.

Regelous, M., A. W. Hofmann, W. Abouchami, and S. J. G. Galer (2003), Geochemistry of lavas from the Emperor Seamounts, and the geochemical evolution of Hawaiian magmatism from 85 to 42 Ma, *J. Petrol.*, *44*(1), 113–140.

Reiners, P. W., and B. K. Nelson (1998), Temporal-compositional-isotopic trends in rejuvenated-stage magmas of Kauai,

Hawaii, and implications for mantle melting processes, *Geochim. Cosmochim. Acta*, *62*(13), 2347–2368.

Roden, M. F., T. Trull, S. R. Hart, and F. A. Frey (1994), New He, Nd, Pb, and Sr isotopic constraints on the constitution of the Hawaiian plume: Results from Koolau Volcano, Oahu, Hawaii, USA, *Geochim. Cosmochim. Acta*, *58*(5), 1431–1440.

Schwandt, C. S., and G. A. McKay (1998), Rare earth element partition coefficients from enstatite/melt synthesis experiments, *Geochim. Cosmochim. Acta*, *62*(16), 2845–2848.

Shafer, J. T., C. R. Neal, and P. R. Castillo (2004), Compositional variability in lavas from the Ontong Java Plateau: Results from basalt clasts within the volcaniclastic succession at Ocean Drilling Program site 1184, in *Origin and Evolution of the Ontong Java Plateau*, edited by J. G. Fitton et al., *Geol. Soc. Spec. Publ.*, *229*, 333–351.

Skulski, T., W. Minarik, and E. B. Watson (1994), High-pressure experimental trace-element partitioning between clinopryoxene and basaltic melts, *Chem. Geol.*, *117*(1–4), 127–147.

Sobolev, A. V., A. A. Migdisov, and M. V. Portnyagin (1996), Incompatible element partitioning between clinopyroxene and basalt liquid revealed by the study of melt inclusions in minerals from Troodos lavas, Cryprus, *Petrology*, *4*(3), 307–317.

Sun, C.-O., R. J. Williams, and S. S. Sun (1974), Distribution coefficients of Eu and Sr for plagioclase-liquid and clinopryoxene-liquid equilibria in oceanic ridge basalt: An experimental study, *Geochim. Cosmochim. Acta*, *38*(9), 1415–1433.

Sun, S., and W. McDonough (1989), Chemical and isotopic systematics of oceanic basalts: Implications for mantle composition and processes, in *Magmatism in the Ocean Basins*, edited by A. Saunders and M. Norry, *Geol. Soc. Spec. Publ.*, *42*, 313–345.

Tarduno, J. A., et al. (Eds.) (2002), *Proceedings of the Ocean Drilling Program, Initial Reports*, vol. 197, Ocean Drill. Program, College Station, Tex.

Villemant, B., H. Jaffrezic, J. L. Joron, and M. Treuil (1981), Distribution coefficients of major and trace elements—Fractional crystallization in the alkali basalt series of Chaine-Des-Puys (Massif Central, France), *Geochim. Cosmochim. Acta*, *45*(11), 1997–2016.

Waight, T. E., J. A. Baker, and B. Willigers (2002), Rb isotope dilution analyses by MC-ICPMS using Zr to correct for mass fractionation: Towards improved Rb-Sr geochronology, *Chem. Geol.*, *186*(1–2), 99–116.

West, H. B., M. O. Garcia, F. A. Frey, and A. K. Kennedy (1988), Nature and cause of compositional variation among the alkalic cap lavas of Mauna Kea Volcano, Hawaii, *Contrib. Mineral. Petrol.*, *100*(3), 383–397.

Wright, T. L. (1984), Origin of Hawaiian tholeiite: A metasomatic model, *J. Geophys. Res.*, *89*(5), 3233–3252.

Yang, H. J., F. A. Frey, and D. A. Clague (2003), Constraints on the source components of lavas forming the Hawaiian North Arch and Honolulu volcanics, *J. Petrol.*, *44*(4), 603–627.

Zindler, A., and E. Jagoutz (1988), Mantle cryptology, *Geochim. Cosmochim. Acta*, *52*, 319–333.